PERGAMON

Computers and Structures 74 (2000) 179–200

Computers & Structures

www.elsevier.com/locate/compstruc

A comprehensive study of a multiplicative elastoplasticity model coupled to damage including parameter identification

Rolf Mahnken*

Institut für Baumechanik und Numerische Mechanik, University of Hannover, Appelstrasse 9a, 30167, Hannover, Germany

Received 25 May 1997; accepted 19 November 1998

Abstract

In this contribution various aspects for a plasticity model coupled to damage are considered. The formulation of the model is performed in the intermediate configuration which occurs as a consequence of the multiplicative decomposition of the deformation gradient. We will resort to thermodynamic consistency, continuous tangent operator, algorithmic tangent operator and sensitivity analysis for parameter identification. Furthermore, for the discretized constitutive problem a robust iteration scheme with a two-level algorithm is proposed. In the numerical example material parameters are determined by least-squares minimization based on experimental data obtained with an optical method.

Keywords: Multiplicative plasticity; Damage; Parameter identification; Two-level local iteration; Linearization; Sensitivity analysis

1. Introduction

The extensive loading of metallic structures leads to degradation of mechanical properties up to complete failure, and this progressive physical process is commonly referred to as damage. Various manifestations of damage have been described in the literature, such as creep damage, low cycle fatigue, high cycle fatigue and brittle damage [1]. The present paper is concerned with isotropic ductile damage, which is induced by large plastic deformations.

Metallographic studies [2,3] demonstrate that ductile damage is basically characterized by three mechanisms of void growth: (i) nucleation of voids due to fracture of particle–matrix interface, failure of the particle or micro-cracking of the matrix surrounding the inclusion; (ii) growth of voids, thus leading to an enlargement of existing holes; and (iii) coalescence or micro-cracks linking neighbouring voids, thus leading to vanishing load carrying capacity of the material, as the void volume fraction approaches unity.

It appears that mainly two different conceptions can be found in the literature in order to model ductile damage effects: *micro-mechanical damage models* and *phenomenological damage models*. A model of the first kind is formulated by Gurson [4], where he derived a yield potential for porous plastic materials from simple cell models. Modifications have been proposed to improve the predictions at low void volume fractions [5] and to provide a better representation of final void coalescence [6]. In this way micro-mechanical models are based on physical soundness, and various applications have modelled void growth and ductile rupture, see e.g. [5–8]. However the identification and determination of the associated micromechanical material parameters is still a rather new approach with no generally accepted recommendations. It can be done by combining metallurgical examinations with cell modelling and macroscopic testing results [8,9].

* Tel.: +49-511-762-2220; fax: +49-511-762-5496.

0045-7949/00/$ - see front matter
PII: S0045-7949(98)00296-X

Phenomenological damage models are based on the concept of Kachanov [10], who was the first to introduce for the isotropic case a one-dimensional variable, which might be interpreted as the effective surface density of microdefects per unit volume ([1], p. 12). The damage variable is combined with the *effective stress concept* in order to relate the effective stresses, acting on the undamaged material, to the nominal stresses, acting on the damaged area. This allows the application of the *strain equivalence principle* in order to formulate constitutive equations in terms of the effective stresses without modifications of known constitutive models (see Lemaitre [1], p. 13ff). Because of the irreversible nature of the damage process thermodynamic concepts have been proposed for the geometric linear case, in which the damage variable is regarded as an internal variable (see e.g. [11–13]). Extensions to the framework of finite deformations are presented e.g. by De Souza et al. [14] or Steinmann et al. [15].

The model of this work is a modification of a previous representation for finite elasto-plasticity described by Miehe [16], whereby in the above-mentioned three approaches are incorporated: (i) a scalar damage variable; (ii) the *effective stress concept*; and (iii) the *strain equivalence principle*. The formulation is obtained relative to the intermediate configuration which occurs as a consequence of the multiplicative decomposition for the deformation gradient into an elastic and a plastic part. The elastic response is formulated in terms of elastic logarithmic strains, where the total elastic part of the free energy is coupled to damage. The choice of a proper dissipation potential leads to rate equations for the evolution of plastic gliding, isotropic hardening and damage. The above-mentioned choice for the coupling of elasticity and damage is regarded as an extension to the formulation of Steinmann et al. [15], where only the isochoric part of the free energy is coupled to damage. As a consequence, the evolution equation for damage is able to simulate the experimental observation that void growth is highly influenced by the triaxiality ratio which is an important feature in the process of the rupture of materials [3,17].

Furthermore thermodynamic consistency of the constitutive relations can be easily verified, and we derive the continuous tangent operator relative to the intermediate configuration, which relates the rate of Mandel stresses to its work conjugate velocity gradient.

The use of an exponential type integration scheme for the flow rule, as proposed by Weber and Anand [18] and Eterovic and Bathe [19] results in a nonlinear problem in the principal directions of the elastic left Cauchy Green trial tensor. This problem can be reduced to a two-dimensional system of equations and is solved with a two-level scheme as proposed by Johansson et al. [20]. The strategy allows the combination of (i) one-dimensional iteration schemes (bisection or pegasus method), which show superior global convergence properties, with (ii) the Newton scheme, which shows only a superior local convergence property.

The additional task of finding the material parameters for the model—which in the mathematical terminology is an inverse problem [21–23]—is based on experimental testing. In classical approaches the specimen is loaded at the heads (force or displacement controlled), and then experimental data are obtained at certain points of the sample assuming *uniform* distribution of all stress or strain quantities within the sample. However, very often the uniformness is difficult to preserve during the experiment (see e.g. Lemaitre [1] p. 22). Therefore, in this contribution spatially distributed data are used, which are obtained with an optical method [24,25]. Then it is the object to minimize the distance of these data to spatially distributed data obtained from finite element computations in a least-squares sense by varying the material parameters. This approach, including the corresponding sensitivity analysis is described e.g. by Mahnken and Stein [26] for the geometric linear theory, and in Mahnken and Stein [27] it has been extended to the geometric nonlinear case based on an algorithm described by Simo [28].

An outline of this work is as follows: in Section 2 the constitutive equations of the damage model by use of tensor quantities relative to the intermediate configuration are summarized. Then thermodynamic consistency of the model is shown and a continuous tangent operator, also relative to the intermediate configuration, is derived. In Section 3 a robust two-level algorithm is proposed, in order to solve the discretized constitutive problem. The algorithmic tangent operator, needed for the application of a Newton-scheme in the equilibrium iteration, and the sensitivity load term, needed for the application of a gradient-based optimization scheme (e.g. Gauss–Newton method, quasi-Newton method) for parameter identification, are derived in Section 4. For illustrative purposes, in Section 5 material parameters are determined by least-squares minimization based on experimental data obtained with an optical method.

1.1. Notations

Square brackets $[\,\cdot\,]$ are used throughout the paper to denote 'function of' in order to distinguish from mathematical groupings with parentheses $(\,\cdot\,)$.

2. Formulation of the model equations

2.1. Notation and kinematics of multiplicative elastoplasticity

Let $\mathscr{B}_0 \subset \mathbb{R}^3$ be the reference configuration of a continuum body **B** with smooth boundary $\partial\mathscr{B}_0$, $\mathscr{I} = [t_0, T] \in \mathbb{R}_+$ the time interval of interest and $\mathscr{K}$ a (vector) space of admissible material parameters. We consider the configuration field $\boldsymbol{\varphi}[\mathbf{X},t,\boldsymbol{\kappa}]$ in terms of the three independent variables $\mathbf{X} \subset \mathscr{B}_0$, $t \subset \mathscr{I}$ and $\boldsymbol{\kappa} \subset \mathscr{K}$. Thus $\boldsymbol{\varphi}[\cdot,t,\boldsymbol{\kappa}]$: $\mathscr{B}_0 \rightarrow \mathbb{R}^3$ defines a nonlinear deformation map at time $t \subset \mathscr{I}$ for given material parameters $\boldsymbol{\kappa} \subset \mathscr{K}$ mapping particles $\mathbf{X} \subset \mathscr{B}_0$ to their actual position $\mathbf{x} \subset \mathscr{B}$ in the deformed configuration. The associated nonlinear deformation gradient $\mathbf{F} = \nabla_X \boldsymbol{\varphi}[\mathbf{X},t,\boldsymbol{\kappa}]$ with $J = \det\mathbf{F}$ defines a mapping of increments $\mathrm{d}\mathbf{X} \subset T\mathscr{B}_0$ of a locally defined tangent space $T\mathscr{B}_0$ associated with the undeformed configuration to increments $\mathrm{d}\mathbf{x} \subset T\mathscr{B}$ of a locally defined tangent space $T\mathscr{B}$ associated with the deformed configuration. Here and if not stated otherwise also in the subsequent presentation, explicit indication of the arguments t and $\boldsymbol{\kappa}$ is omitted. Furthermore we endow the tangent spaces $T\mathscr{B}_0$ and $T\mathscr{B}$ with co-variant metric tensors $\mathbf{G}^\flat$ and $\mathbf{g}^\flat$, respectively.

The time and parameter derivatives of the configuration field are denoted by $\dot{\boldsymbol{\varphi}} = \partial_t\boldsymbol{\varphi}$ and $\partial_{\boldsymbol{\kappa}}\boldsymbol{\varphi}$, respectively. For the subsequent representation, we will also introduce kinematic expressions by replacing the time derivative $\partial_t(\,\cdot\,)$ or the parameter derivative $\partial_{\boldsymbol{\kappa}}(\cdot)$ by its variational counterparts $\partial_\delta(\,\cdot\,)$ and $\partial_\Delta(\,\cdot\,)$, respectively, where now $\partial_\delta(\,\cdot\,)$ and $\partial_\Delta(\,\cdot\,)$ are short-hand notations for the Gâteaux derivative at the point $\mathbf{x} = \boldsymbol{\varphi}(\mathbf{X},t,\boldsymbol{\kappa})$ in the direction of the virtual variation $\delta\mathbf{u}$ and increment for linearization $\Delta\mathbf{u}$, respectively. With the above notation different kinematic variables and associated derivatives can be defined [27]. Some examples for velocity gradients, rate of deformation tensors and Lie derivative operators are as follows:

$$\mathbf{l} = \nabla_{\mathbf{x}}\partial_t\boldsymbol{\varphi} \quad \mathbf{d} = \mathrm{sym}(\mathbf{g}^\flat \cdot \mathbf{l})$$

$$\mathscr{L}^{\#}_t(\cdot) = \mathbf{F}\cdot\partial_t(\mathbf{F}^{-1}\cdot(\cdot)^{\#}\cdot\mathbf{F}^{-\mathrm{t}})\cdot\mathbf{F}^{\mathrm{t}}$$

$$\mathscr{L}^{\flat}_t(\cdot) = \mathbf{F}^{-\mathrm{t}}\cdot\partial_t(\mathbf{F}^{\mathrm{t}}\cdot(\cdot)^{\flat}\cdot\mathbf{F})\cdot\mathbf{F}^{-1}$$

$$\mathbf{l}_{\boldsymbol{\kappa}} = \nabla_{\mathbf{x}}\partial_{\boldsymbol{\kappa}}\boldsymbol{\varphi} \quad \mathbf{d}_{\boldsymbol{\kappa}} = \mathrm{sym}(\mathbf{g}^\flat \cdot \mathbf{l}_{\boldsymbol{\kappa}})$$

$$\mathscr{L}^{\#}_{\boldsymbol{\kappa}}(\cdot) = \mathbf{F}\cdot\partial_{\boldsymbol{\kappa}}(\mathbf{F}^{-1}\cdot(\cdot)^{\#}\cdot\mathbf{F}^{-\mathrm{t}})\cdot\mathbf{F}^{\mathrm{t}}$$

$$\mathscr{L}^{\flat}_{\boldsymbol{\kappa}}(\cdot) = \mathbf{F}^{-\mathrm{t}}\cdot\partial_{\boldsymbol{\kappa}}(\mathbf{F}^{\mathrm{t}}\cdot(\cdot)^{\flat}\cdot\mathbf{F})\cdot\mathbf{F}^{-1}$$

$$\mathbf{l}_\delta = \nabla_{\mathbf{x}}\partial_\delta\boldsymbol{\varphi} \quad \mathbf{d}_\delta = \mathrm{sym}(\mathbf{g}^\flat \cdot \mathbf{l}_\delta)$$

$$\mathscr{L}^{\#}_\delta(\cdot) = \mathbf{F}\cdot\partial_\delta(\mathbf{F}^{-1}\cdot(\cdot)^{\#}\cdot\mathbf{F}^{-\mathrm{t}})\cdot\mathbf{F}^{\mathrm{t}}$$

$$\mathscr{L}^{\flat}_\delta(\cdot) = \mathbf{F}^{-\mathrm{t}}\cdot\partial_\delta(\mathbf{F}^{\mathrm{t}}\cdot(\cdot)^{\flat}\cdot\mathbf{F})\cdot\mathbf{F}^{-1}$$

$$\mathbf{l}_\Delta = \nabla_{\mathbf{x}}\partial_\Delta\boldsymbol{\varphi} \quad \mathbf{d}_\Delta = \mathrm{sym}(\mathbf{g}^\flat \cdot \mathbf{l}_\Delta)$$

$$\mathscr{L}^{\#}_\Delta(\cdot) = \mathbf{F}\cdot\partial_\Delta(\mathbf{F}^{-1}\cdot(\cdot)^{\#}\cdot\mathbf{F}^{-\mathrm{t}})\cdot\mathbf{F}^{\mathrm{t}} \tag{1}$$

$$\mathscr{L}^{\flat}_\Delta(\cdot) = \mathbf{F}^{-\mathrm{t}}\cdot\partial_\Delta(\mathbf{F}^{\mathrm{t}}\cdot(\cdot)^{\flat}\cdot\mathbf{F})\cdot\mathbf{F}^{-1}$$

where $(\,\cdot\,)^{\#}$ and $(\,\cdot\,)^{\flat}$ denote a contra-variant and co-variant tensor object, respectively. The underlying concept of multiplicative elastoplasticity assumes the decomposition

$$\mathbf{F} = \mathbf{F}_{\mathrm{e}}\cdot\mathbf{F}_{\mathrm{p}} \tag{2}$$

where $\mathbf{F}_{\mathrm{e}}$ and $\mathbf{F}_{\mathrm{p}}$ represent the elastic and plastic part of **F**, respectively, and which implies a plastic intermediate configuration $\mathscr{B}_{\mathrm{p}}$ as macro stress free. Based on the assumption (2) an elastic pull-back of the velocity gradient $\mathbf{l} = \dot{\mathbf{F}}\cdot\mathbf{F}^{-1} = \dot{\mathbf{F}}_{\mathrm{e}}\cdot\mathbf{F}_{\mathrm{e}}^{-1} + \mathbf{F}_{\mathrm{e}}\cdot\dot{\mathbf{F}}_{\mathrm{p}}\cdot\mathbf{F}_{\mathrm{p}}^{-1}\cdot\mathbf{F}_{\mathrm{e}}^{-1}$ yields for the velocity gradient relative to the intermediate configuration $\bar{\mathbf{L}} = \mathbf{F}_{\mathrm{e}}^{-1}\cdot\mathbf{l}\cdot\mathbf{F}_{\mathrm{e}}$ with additive decomposition

$$\bar{\mathbf{L}} = \bar{\mathbf{L}}_{\mathrm{e}} + \bar{\mathbf{L}}_{\mathrm{p}} \tag{3a}$$

where

$$\bar{\mathbf{L}}_{\mathrm{e}} := \mathbf{F}_{\mathrm{e}}^{-1}\cdot\dot{\mathbf{F}}_{\mathrm{e}} \tag{3b}$$

and

$$\bar{\mathbf{L}}_{\mathrm{p}} := \dot{\mathbf{F}}_{\mathrm{p}}\cdot\mathbf{F}_{\mathrm{p}}^{-1} \tag{3c}$$

As noted by Miehe [16], this decoupled representation for the evolution of elastic and plastic deformation is possible within a geometric setting relative to the intermediate configuration in terms of mixed-variant (contra-covariant) tensor fields $\bar{\mathbf{L}}_{\mathrm{e}}$ and $\bar{\mathbf{L}}_{\mathrm{p}}$.

In what follows we will also consider the elastic right Cauchy–Green tensor defined on the intermediate configuration

$$\mathbf{C}_{\mathrm{e}} = \mathbf{F}_{\mathrm{e}}^{\mathrm{t}}\cdot\mathbf{g}^\flat\cdot\mathbf{F}_{\mathrm{e}} \tag{4}$$

and the multiplicative split

$$\mathbf{C}_{\mathrm{e}} = J_{\mathrm{e}}^{2/3}\hat{\mathbf{C}}_{\mathrm{e}}, \quad \text{where} \quad J_{\mathrm{e}} = (\det\,\mathbf{C}_{\mathrm{e}})^{1/2} \tag{5}$$

Consequently $\hat{\mathbf{C}}_{\mathrm{e}}$ and J_{e} represent the isochoric and volumetric part of the elastic deformation, respectively.

2.2. Free energy and thermodynamic forces

The starting point for a thermodynamic consistent model suitable for ductile materials is the following Helmholtz free energy:

$$\Psi = (1-\alpha)\Psi^{\mathrm{el}}[\mathbf{C}_{\mathrm{e}}] + \Psi^{\mathrm{p}}[q] \tag{6a}$$

where

$$\Psi^{\mathrm{el}} = \Psi^{\mathrm{vol}}[J_{\mathrm{e}}] + \Psi^{\mathrm{iso}}[\hat{\mathbf{C}}_{\mathrm{e}}] \tag{6b}$$

$$\Psi^{\mathrm{vol}} = \tfrac{1}{2}K(\ln\ J_{\mathrm{e}})^2 \tag{6c}$$

$$\Psi^{\mathrm{iso}} = \frac{G}{4}(\mathrm{tr}(\ln\ \hat{\mathbf{C}}_{\mathrm{e}})^2) \tag{6d}$$

$$\Psi^{\mathrm{p}} = c\left(q + \frac{1}{b}\exp(-bq)\right) \tag{6e}$$

Here the decoupled form for the elastic part is based on the volumetric-isochoric split, Eq. (5), for the elastic right Cauchy–Green tensor with corresponding bulk modulus K and shear modulus G, respectively. The damage variable α represents local degradation of the elastic properties, and q is a strain-like internal variable describing the state of the material at the micro level induced by dislocations with associated material parameters c and b. The above formulation is the analog of the Helmholtz free energy within a geometrically linear 'state kinetic coupling theory' formulated by Lemaitre ([1], p. 42). In particular, state coupling of damage with elastic strain as shown experimentally is assumed, but there is no state coupling either between plasticity and elasticity or between damage and plasticity. The formulation (6e) gives the classical expression for isotropic hardening with saturation for large plastic strain.

Thermodynamnic formulations for isothermal processes are based on the principle of positive dissipation

$$\mathscr{D} = \mathscr{P} - \dot{\Psi} \geq 0 \tag{7}$$

Using tensor quantities relative to the actual configuration the stress-power is given as a dual pairing $\mathscr{P} = \boldsymbol{\tau}:\mathbf{d}$ with the (contravariant) Kirchhoff stress tensor $\boldsymbol{\tau}$ and the (covariant) spatial rate of deformation tensor $\mathbf{d} = \mathrm{sym}(\mathbf{g}^{\flat} \cdot \mathbf{l})$, whereas with tensor quantities relative to the reference configuration we have $\mathscr{P} = \mathbf{S}:\mathbf{D}$ in terms of the (contravariant) second Piola–Kirchhoff stress tensor $\mathbf{S} = \mathbf{F}^{-1} \cdot \boldsymbol{\tau} \cdot \mathbf{F}^{-\mathrm{t}}$ and a (covariant) material rate of deformation tensor $\mathbf{D} = \mathbf{F}^{\mathrm{t}} \cdot \mathbf{d} \cdot \mathbf{F} = \mathrm{sym}(\dot{\mathbf{F}}^{\mathrm{t}} \cdot \mathbf{F})$. Following Miehe [16], alternatively the stress power can be written relative to the intermediate configuration as $\mathscr{P} = \bar{\mathbf{T}}:\bar{\mathbf{L}}$, where $\bar{\mathbf{T}} = \mathbf{F}_{\mathrm{e}}^{\mathrm{t}} \cdot \mathbf{g}^{\flat} \cdot \boldsymbol{\tau} \cdot \mathbf{F}_{\mathrm{e}}^{-\mathrm{t}}$ is the mixed variant (co-contravariant) Mandel stress tensor, and $\bar{\mathbf{L}}$ is the total velocity gradient introduced in the previous section. Consequently, using the additive decomposition, Eqs. (3a)–(3c), and the identity $\partial\Psi/\partial\mathbf{C}_{\mathrm{e}}:\dot{\mathbf{C}}_{\mathrm{e}} = 2(\mathbf{C}_{\mathrm{e}} \cdot \partial\Psi/\partial\mathbf{C}_{\mathrm{e}}):\bar{\mathbf{L}}_{\mathrm{e}}$ the dissipation (7) results into

$$\mathscr{D} = \left[\bar{\mathbf{T}} - 2\mathbf{C}_{\mathrm{e}} \cdot \frac{\partial\Psi}{\partial\mathbf{C}_{\mathrm{e}}}\right]:\bar{\mathbf{L}} + 2\mathbf{C}_{\mathrm{e}} \cdot \frac{\partial\Psi}{\partial\mathbf{C}_{\mathrm{e}}}:\bar{\mathbf{L}}_{\mathrm{p}} - \frac{\partial\Psi}{\partial q}\dot{q} - \frac{\partial\Psi}{\partial\alpha}\dot{\alpha} \geq 0 \tag{8}$$

Employing the standard argument of thermodynamics, that the above relation holds for all processes $\bar{\mathbf{L}}$, implies $\bar{\mathbf{T}} = 2\mathbf{C}_{\mathrm{e}} \cdot \partial\Psi/\partial\mathbf{C}_{\mathrm{e}}$ and thus for the logarithmic model, Eqs. (6a)–(6c) it follows:

$$\bar{\mathbf{T}} = (1-\alpha)\hat{\bar{\mathbf{T}}}, \quad \text{with} \quad \hat{\bar{\mathbf{T}}} = \hat{\bar{\mathbf{T}}}^{\mathrm{vol}} + \hat{\bar{\mathbf{T}}}^{\mathrm{iso}} \quad \text{and} \tag{9a}$$

$$\hat{\bar{\mathbf{T}}}^{\mathrm{vol}} = p\mathbf{1}, \quad p = K\ \ln\ J_{\mathrm{e}} \tag{9b}$$

$$\hat{\bar{\mathbf{T}}}^{\mathrm{iso}} = G\ \ln\ \hat{C}_{\mathrm{e}} = G\,\mathrm{dev}\ln\mathbf{C}_{\mathrm{e}} = \hat{\bar{\mathbf{T}}}^{\mathrm{dev}} \tag{9c}$$

The relations (9a)–(9c) express the *effective stress concept* (see Lemaitre [1], p. 42), thus relating the 'nominal' Mandel stress tensor $\bar{\mathbf{T}}$ to the effective Mandel stress tensor $\hat{\bar{\mathbf{T}}}$ acting on the remaining undamaged material.

For subsequent purposes we define the hardening variable Q and the damage energy release rate A as the thermodynamic forces conjugate to the internal variables q and α as

$$Q = \frac{\partial\Psi}{\partial q} = c(1 - \exp(-bq))$$

$$A = \frac{\partial\Psi}{\partial\alpha} = -\frac{p^2}{2K} - \frac{1}{4G}\|\hat{\bar{\mathbf{T}}}^{\mathrm{dev}}\|^2 \tag{10}$$

Here the relations $\Psi^{\mathrm{vol}} = (1/2)K(\ln\ J_{\mathrm{e}})^2 = p^2/(2\ K)$ and $\Psi^{\mathrm{iso}} = (1/4)G\mathrm{tr}(\ln\ \hat{\mathbf{C}}_{\mathrm{e}})^2 = \|\hat{\bar{\mathbf{T}}}^{\mathrm{dev}}\|^2/(4G)$ have been exploited.

2.3. Dissipation potential and evolution of internal variables

In order to describe plasticity of ductile materials a separate potential of dissipation $\Phi*$ is introduced depending on the effective Mandel stress $\hat{\bar{\mathbf{T}}}$, the hardening variable Q and the damage energy release rate A as a sum of two functions

$$\Phi^* = \Phi_{\mathrm{p}}^*[\hat{\bar{\mathbf{T}}}, Q] + \Phi_{\mathrm{d}}^*[A] \tag{11}$$

Note, that the formulation for Φ_{p}^{*} is in accordance with the *principle of strain equivalence*, whereby the yield criterion is written in the same way as for the nondamaged material except that the stress tensor $\bar{\mathbf{T}}$ is replaced by the effective stress tensor $\hat{\bar{\mathbf{T}}}$. For definiteness we choose for the plastic potential Φ_{p}^{*} and the damage potential Φ_{d}^{*}

$$\Phi_{\mathrm{p}}^{*}=\|\hat{\bar{\mathbf{T}}}^{\mathrm{dev}}\|-\sqrt{\frac{2}{3}}(Y_0+Q)$$

$$\Phi_{\mathrm{d}}^{*}=\frac{(-A)^2}{2S(1-\alpha)^m}\mathscr{T}[q] \tag{12}$$

where the threshold function $\mathscr{T}[q]$ has been introduced, in order to activate damage only if a certain limit ϵ_1 has been obtained for q (see Lemaitre [1], p. 96). A possible choice for $\mathscr{T}$ is the Hermitian polynomial

$$\mathscr{T}[q;\epsilon_1,\epsilon_2]=0 \quad \text{if} \quad q\le\epsilon_1$$

$$\mathscr{T}[q;\epsilon_1,\epsilon_2]=\frac{(q-\epsilon_1)^2}{(\epsilon_2-\epsilon_1)^2}\left(3-2\frac{q-\epsilon_1}{\epsilon_2-\epsilon_1}\right) \quad \text{if} \quad \epsilon_1<q<\epsilon_2$$

$$\mathscr{T}[q;\epsilon_1,\epsilon_2]=1 \quad \text{if} \quad \epsilon_2\le q \tag{13}$$

which due to its smoothness is of advantage for the numerical implementation, see Johansson et al. [20]. It follows that ϵ_1,ϵ_2 can be regarded as material parameters.

The evolution for the set of internal variables $[\bar{\mathbf{L}}_{\mathrm{p}},\dot{q},\dot{\alpha}]$ is now proposed based on the principle of generalized normalities as

$$\bar{\mathbf{L}}_{\mathrm{p}}=\dot{\lambda}\frac{\partial\Phi^{*}}{\partial\bar{\mathbf{T}}}=\frac{\dot{\lambda}}{1-\alpha}\bar{\mathbf{M}}, \quad \text{where}$$
$$\bar{\mathbf{M}}=\frac{\partial\Phi_{\mathrm{p}}^{*}}{\partial\hat{\bar{\mathbf{T}}}}=\frac{(\hat{\bar{\mathbf{T}}}^{\mathrm{dev}})^{\mathrm{t}}}{\|\hat{\bar{\mathbf{T}}}^{\mathrm{dev}}\|} \tag{14a}$$

$$\dot{q}=-\dot{\lambda}\frac{\partial\Phi^{*}}{\partial Q}=-\dot{\lambda}M_q, \quad \text{where}$$
$$M_q=\frac{\partial\Phi_{\mathrm{p}}^{*}}{\partial Q}=-\sqrt{\frac{2}{3}} \tag{14b}$$

$$\dot{\alpha}=-\dot{\lambda}\frac{\partial\Phi^{*}}{\partial A}=-\dot{\lambda}M_{\alpha}, \quad \text{where}$$
$$M_{\alpha}=\frac{\partial\Phi_{d}^{*}}{\partial A}=\frac{A}{S(1-\alpha)^m}\mathscr{T}[q] \tag{14c}$$

The scalar $\dot{\lambda}$ is the plastic multiplier obtained from the loading and unloading conditions

$$\dot{\lambda}\ge 0$$

$$\Phi_Y\le 0$$

$$\dot{\lambda}\Phi_Y=0 \tag{15}$$

where Φ_Y is the yield function. In the simplest case we set

$$\Phi_Y=\Phi_{\mathrm{p}}^{*}=\|\hat{\bar{\mathbf{T}}}^{\mathrm{dev}}\|-\sqrt{\frac{2}{3}}(Y_0+Q) \tag{16}$$

Remark 1. Note, that due to the choices, Eq. (12), the above evolution equations (14a)–(14c) exhibit an associated flow rule for the evolution of plastic flow and hardening evolution but a nonassociative flow rule for the damage evolution.

Remark 2. The evolution rule α specified by Eq. (14c) predicts the rate of α to be proportional to the conjugate thermodynamic force A. This implies the identical growth of α for both positive and negative hydrostatic stress. However for certain materials (e.g. brittle materials) and certain loading conditions the defect may close in compression and reopen in tension. Following Lemaitre [1], this 'microcrack closure reopening' (MCR) effect can be incorporated into the above constitutive equations by a straightforward modification. An example within the geometric linear setting is proposed by Johansson et al. [20].

Remark 3. Upon defining the invariants

$$\sigma_{\mathrm{v}}:=\sqrt{\frac{3}{2}}\|\bar{\mathbf{T}}^{\mathrm{dev}}\|$$

$$\sigma_{\mathrm{h}}:=\frac{1}{3}\mathrm{tr}(\bar{\mathbf{T}})$$

$$\dot{e}_{\mathrm{v}}:=\sqrt{\frac{2}{3}}\|\bar{\mathbf{L}}_{\mathrm{p}}\| \tag{17}$$

for the Mandel stress tensor and the plastic part of the velocity gradient relative to the intermediate configuration, the evolution equation for the damage variable (14c) can be rewritten as

$$\dot{\alpha}=-\dot{e}_{\mathrm{v}}\frac{\bar{A}}{S(1-\alpha)^{(m-1)}}\mathscr{T}[q]$$

where

$$\bar{A} = -\frac{\sigma_v^2}{(1-\alpha)^2}\left(\frac{1}{2K}\frac{\sigma_h^2}{\sigma_v^2} + \frac{1}{6G}\right) \tag{18}$$

The presentation (18) reveals that evolution of damage is proportional to the accumulated plastic strain rate $\dot{e}_v$, which is in accordance with the analytical investigations for ductile growth of voids by Rice and Tracey [17]. Furthermore, as noted by Lemaitre ([1], p. 44 and p. 97), the triaxiality ratio σ_h/σ_v, plays a very important role in the rupture of materials (see also Rice and Tracey [17]). The presentation (18) shows an increase of damage evolution with increasing σ_h/σ_v, which is in agreement with the experimental observation, that the measured ductility at fracture decreases as the triaxiality ratio increases [2,3]. In this respect the formulation (14c) is regarded as an important modification to the formulation presented by Steinmann et al. [15], and, as it will be seen later, has some consequences in the numerical implementation. Lastly we note that, due to the factors $(1-\alpha)$ in the denominators of the presentation (18), an increase of damage evolution with increasing α is obtained for $m > 0$.

2.4. Thermodynamic consistency

According to the second law of thermodynamics the dissipation inequality (7) must be satisfied for the evolution equations (14a)–(14c). Here only the loading case $\dot{\lambda} > 0$, $\Phi_Y = 0$ shall be considered, since the unloading case with $\dot{\lambda} = 0$ is trivial. Combining the relations (14a)–(14c), (10), (8) entails writing

$$\begin{aligned}\mathscr{D} &= \bar{\mathbf{T}}:\bar{\mathbf{L}}_p - Q\dot{q} - A\dot{\alpha} \\ &= \dot{\lambda}\left(\frac{1-\alpha}{1-\alpha}\hat{\bar{\mathbf{T}}}^{\mathrm{dev}}:\frac{\hat{\bar{\mathbf{T}}}^{\mathrm{dev}}}{\|\hat{\bar{\mathbf{T}}}^{\mathrm{dev}}\|} - Q\sqrt{\frac{2}{3}} + \frac{A^2}{S(1-\alpha)^m}\mathscr{T}(q)\right) \\ &= \dot{\lambda}\left(\sqrt{\frac{2}{3}}Y_0 + \frac{A^2}{S(1-\alpha)^m}\mathscr{T}(q)\right) > 0\end{aligned}$$

The last relation is obtained from the yield function (16) for the case of loading with $\Phi_Y = 0$.

2.5. Summary of material parameters

We are now in a position to summarize all material constants of the model, characterizing the inelastic behavior, which, apart from the elastic constants K and G, have to be calibrated based on experimental data

$$\boldsymbol{\kappa} = [Y_0, c, b, S, m, \epsilon_1, \epsilon_2]^t \tag{19}$$

In order to be physically meaningful the material parameters are restricted to lower and upper bounds a_i, b_i, respectively. These constraints then define the feasible domain $\mathscr{K}$, such that

$$\boldsymbol{\kappa} \in \mathscr{K} \subset \mathbb{R}^{n_p}$$

$$\mathscr{K} := \{\boldsymbol{\kappa} : a_i \le \kappa_i \le b_i, i = 1, \ldots, n_p\} \tag{20}$$

where $n_p = \dim(\boldsymbol{\kappa}) = 7$ denotes the number of material parameters.

2.6. Continuous tangent operator

Continuous consistent tangent operators relate time derivatives of some stress tensor to its work conjugate rate of deformation tensor. In the framework of multiplicative plasticity these relations, which can be regarded as counterparts of so-called *Prandtl–Reuss tensors* of the geometric linear theory, have been firstly derived by Miehe [16] for associative flow rules without hardening and furthermore by Steinmann [29], where additionally damage has been taken into account. In what follows we will derive an operator $\mathscr{A}_0^{pl}$, which relates the time derivative of Mandel stresses $\bar{\mathbf{T}}$ to the velocity gradient $\bar{\mathbf{L}}$ relative to the intermediate configuration as

$$\dot{\bar{\mathbf{T}}} = \mathscr{A}_0^{pl}:\bar{\mathbf{L}}^t \tag{21}$$

Starting with $\hat{\bar{\mathbf{T}}} = 2\mathbf{C}_e \cdot \partial\Psi^{el}/\partial\mathbf{C}_e$ and using the relation $\dot{\mathbf{C}}_e = \mathrm{sym}(\mathbf{C}_e \cdot \bar{\mathbf{L}}_e)$ the total time derivative of the effective Mandel stress is

$$\dot{\hat{\bar{\mathbf{T}}}} = \mathscr{A}_0^{el}:\bar{\mathbf{L}}_e^t$$

where $\mathscr{A}_0^{el} = \mathscr{A}_2^{el} + \mathbf{I}\otimes\hat{\bar{\mathbf{T}}}^t + \mathbf{C}_e\underline{\otimes}\hat{\bar{\mathbf{T}}}^t \cdot \mathbf{C}_e^{-1}$

$$\mathscr{A}_2^{el} = \mathbf{C}_e \cdot \bar{\mathbb{C}} \cdot \mathbf{C}_e$$

$$\bar{\mathbb{C}} = 4\frac{\partial^2\Psi^{el}}{\partial\mathbf{C}_e\partial\mathbf{C}_e} \tag{22}$$

which defines a fourth-order hyperelastic tensor $\mathscr{A}_0^{el}$. (Here $\otimes$ and $\underline{\otimes}$ define non-standard tensor products such that $(\mathbf{a}\otimes\mathbf{b}):\mathbf{c} = \mathbf{a}\cdot\mathbf{c}\cdot\mathbf{b}^t$, $(\mathbf{a}(\underline{\otimes})\mathbf{b}):\mathbf{c} = \mathbf{a}\cdot\mathbf{c}^t\cdot\mathbf{b}^t$, see e.g. Steinmann [29].) Likewise, the time derivatives of the stress like internal variables are

$$\dot{Q} = -\dot{\lambda}H_q M_q, \quad \text{where } H_q = \frac{\partial^2\Psi}{\partial q\partial q}$$

$$\dot{A} = -\dot{\lambda} H_\alpha M_\alpha, \quad \text{where } H_\alpha = \frac{\partial^2 \Psi}{\partial \alpha \partial \alpha} \tag{23}$$

Upon introducing the definitions

$$\bar{\mathbf{N}} = \frac{\partial \Phi_Y}{\partial \hat{\bar{\mathbf{T}}}} \tag{24a}$$

$$N_q = \frac{\partial \Phi_Y}{\partial Q} \tag{24b}$$

$$N_\alpha = \frac{\partial \Phi_Y}{\partial A} \tag{24c}$$

and combining the relations (22) and (23) and $\bar{\mathbf{L}}_e \overset{=}{=} \bar{\mathbf{L}} - \dot{\lambda}/(1-\alpha)\bar{\mathbf{M}}$ the consistency condition $\dot{\Phi}_Y = \bar{\mathbf{N}}:\dot{\hat{\bar{\mathbf{T}}}} + N_q \dot{Q} + N_\alpha \dot{A} = 0$ yields the plastic multiplicator as

$$\dot{\lambda} = \frac{1}{h}\bar{\mathbf{N}}:\mathscr{A}_0^{\mathrm{el}}:\bar{\mathbf{L}}^{\mathrm{t}}, \quad \text{where}$$
$$h = \frac{1}{1-\alpha}\bar{\mathbf{N}}:\mathscr{A}_0^{\mathrm{el}}:\bar{\mathbf{M}} + N_q H_q M_q + N_\alpha H_\alpha M_\alpha \tag{25}$$

From Eq. (9a) it follows

$$\dot{\hat{\bar{\mathbf{T}}}} = (1-\alpha)\dot{\hat{\bar{\mathbf{T}}}} - \hat{\bar{\mathbf{T}}}\,\dot{\alpha} \tag{26}$$

which combined with Eqs. (14c), (22) and (25) yields the hyperelastic–plastic tangent operator in the intermediate configuration as

$$\mathscr{A}_0^{\mathrm{pl}} = (1-\alpha)\mathscr{A}_0^{\mathrm{el}} - \frac{1}{h}(\mathscr{A}_0^{\mathrm{el}}:\bar{\mathbf{M}}^{\mathrm{t}} + \hat{\bar{\mathbf{T}}}\, M_\alpha) \otimes \bar{\mathbf{N}}:\mathscr{A}_0^{\mathrm{el}} \tag{27}$$

and which in the general case exhibits a nonsymmetric structure.

For the logarithmic model, Eqs. (6a)–(6e), use of the relations (see e.g. Steinmann [29])

$$\dot{\overline{\ln J_e}} = \mathbf{1}:\bar{\mathbf{L}}_e^{\mathrm{t}}$$

$$\dot{\overline{\mathrm{tr} \ln \mathbf{C}_e}} = 2\mathbf{1}:\bar{\mathbf{L}}_e^{\mathrm{t}} \tag{28}$$

expands the elastic operator $\mathscr{A}_0^{\mathrm{el}}$ from Eqs. (9a)–(9c) as

$$\mathscr{A}_0^{\mathrm{el}} = \mathscr{A}_0^{\mathrm{el,vol}} + \mathscr{A}_0^{\mathrm{el,dev}}, \quad \text{where } \mathscr{A}_0^{\mathrm{el,vol}} = K\mathbf{1} \otimes \mathbf{1}$$

$$\mathscr{A}_0^{\mathrm{el,dev}} = 2G\left[\frac{\partial\ \ln\ \mathbf{C}_e}{\partial \mathbf{C}_e} \cdot \mathbf{C}_e - \frac{1}{3}\mathbf{1} \otimes \mathbf{1}\right] \tag{29}$$

Furthermore, for isotropy we have $\bar{\mathbf{N}}:\mathscr{A}_0^{\mathrm{el}}:\bar{\mathbf{L}}_e^{\mathrm{t}} = G\bar{\mathbf{N}}:\dot{\overline{\ln\ \mathbf{C}_e}} = 2G\bar{\mathbf{N}}:\bar{\mathbf{L}}_e^{\mathrm{t}}$ and thus $\bar{\mathbf{N}}:\mathscr{A}_0^{\mathrm{el}} = 2G\bar{\mathbf{N}}$ and $\bar{\mathbf{N}}:\mathscr{A}_0^{\mathrm{el}}:\bar{\mathbf{N}} = 2G$. From this, Eq. (27) reveals the hyperelastic–plastic tangent operator for the logarithmic model as

$$\mathscr{A}_0^{\mathrm{pl}} = (1-\alpha)\mathscr{A}_0^{\mathrm{el}} - \frac{2G}{h}(2G + \|\hat{\bar{\mathbf{T}}}\|M_\alpha)\bar{\mathbf{N}} \otimes \bar{\mathbf{N}} \tag{30}$$

Note, that due to the associative flow rule, the above operator shows a symmetric structure.

3. Numerical implementation

3.1. Integration scheme

In this section the numerical integration of the evolution equations (14a)–(14c) is described over a finite time step $\Delta t = {}^{n+1}t - {}^{n}t$ for given initial data ${}^{n}q$, ${}^{n}\alpha$, ${}^{n}\mathbf{C}_{\mathrm{p}}^{-1}$ and deformation gradient ${}^{n+1}\mathbf{F}$, where ${}^{n}\mathbf{C}_{\mathrm{p}} = {}^{n}\mathbf{F}_{\mathrm{p}}^{\mathrm{t}} \cdot {}^{n}\mathbf{F}_{\mathrm{p}}$ is a plastic right Cauchy–Green strain tensor. The starting point for numerical integration of the flow rule, Eq. (14a) is the representation

$$\bar{\mathbf{L}}_{\mathrm{p}} = \dot{\mathbf{F}}_{\mathrm{p}} \cdot \mathbf{F}_{\mathrm{p}}^{-1} = \frac{\dot{\lambda}}{1-\alpha}\bar{\mathbf{M}}$$

$$\bar{\mathbf{M}} = \bar{\mathbf{N}} \rightsquigarrow \dot{\mathbf{F}}_{\mathrm{p}} = \frac{\dot{\lambda}}{1-\alpha}\bar{\mathbf{N}} \cdot \mathbf{F}_{\mathrm{p}} \tag{31}$$

where the relations (3c), (14a), (24a) and (16) have been combined. Then, using an exponential type of integration rule for $\mathbf{F}_{\mathrm{p}}$ [18,19] and a backward Euler scheme for q and α we have

$${}^{n+1}\mathbf{F}_{\mathrm{p}} = \exp\left(\frac{\Delta\lambda}{1-\alpha}\bar{\mathbf{N}}\right) \cdot {}^{n}\mathbf{F}_{\mathrm{p}} \tag{32a}$$

$${}^{n+1}q = {}^{n}q + \Delta\lambda\sqrt{\tfrac{2}{3}} \tag{32b}$$

$${}^{n+1}\alpha = {}^{n}\alpha - \Delta\lambda\frac{{}^{n+1}A}{S(1-\alpha)^m}\mathscr{T}[{}^{n+1}q] \tag{32c}$$

From now on, if confusion is out of danger we will neglect the index $n+1$ referring to the actual time step. Then, we introduce the following 'trial' quantities

$$\mathbf{F}^{\mathrm{tr}} = \mathbf{F} \cdot {}^{n}\mathbf{F}_{\mathrm{p}}^{-1} \rightsquigarrow \mathbf{C}^{\mathrm{tr}} = \mathbf{F}^{\mathrm{tr}^{\mathrm{t}}} \cdot \mathbf{F}^{\mathrm{tr}} \rightsquigarrow \mathbf{C}_{\mathrm{e}}$$
$$= \mathbf{F}_{\mathrm{e}}^{\mathrm{t}} \cdot \mathbf{F}_{\mathrm{e}} = \exp\left(\frac{-\Delta\lambda}{1-\alpha}\bar{\mathbf{N}}\right) \cdot \mathbf{C}^{\mathrm{tr}}$$
$$\cdot \exp\left(\frac{-\Delta\lambda}{1-\alpha}\bar{\mathbf{N}}\right) \tag{33}$$

Using the fact, that $\mathbf{C}_{\mathrm{e}}$, $\mathbf{C}^{\mathrm{tr}}$ and $\bar{\mathbf{N}}$ commute (i.e. have identical principal axes) and decomposing the logarithmic part of $\mathbf{C}_{\mathrm{e}}$ into its deviatoric and its volumetric part yields

$$\ln\ \hat{\mathbf{C}}_{\mathrm{e}} = \ln\ \hat{\mathbf{C}}^{\mathrm{tr}} - \frac{2\Delta\lambda}{1-\alpha}\bar{\mathbf{N}}$$

where $\hat{\mathbf{C}}^{\mathrm{tr}} = (J^{\mathrm{tr}})^{-2/3}\mathbf{C}^{\mathrm{tr}}$

$$J^{\mathrm{tr}} = \det(\mathbf{F}^{\mathrm{tr}})$$

$$\ln\ J_{\mathrm{e}} = \ln\ J^{\mathrm{tr}} \tag{34}$$

Then, by use of Eqs. (9a)–(9c), the Mandel stresses are decomposed as

$$\mathbf{T} = (1-\alpha)\hat{\bar{\mathbf{T}}}, \quad \text{with } \hat{\bar{\mathbf{T}}} = \hat{\bar{\mathbf{T}}}^{\mathrm{vol}} + \hat{\bar{\mathbf{T}}}^{\mathrm{dev}} \text{ and}$$

$$\hat{\bar{\mathbf{T}}}^{\mathrm{vol}} = p\mathbf{1}, \quad p = K\ \ln\ J^{\mathrm{tr}}$$

$$\hat{\bar{\mathbf{T}}}^{\mathrm{dev}} = \hat{\bar{\mathbf{T}}}^{\mathrm{dev,tr}} - \frac{2G\Delta\lambda}{1-\alpha}\bar{\mathbf{N}}, \quad \text{where } \hat{\bar{\mathbf{T}}}^{\mathrm{dev,tr}} = G\ln\hat{\mathbf{C}}^{\mathrm{tr}} \tag{35}$$

A more advantageous formulation for the finite element implementation is obtained relative to the actual configuration with the Kirchhoff stresses $\boldsymbol{\tau} = \mathbf{g}^{\#}\cdot\mathbf{F}_{\mathrm{e}}^{-\mathrm{t}}\cdot\bar{\mathbf{T}}\cdot\mathbf{F}_{\mathrm{e}}^{\mathrm{t}}$. Thus, by use of the left Cauchy–Green trial tensor

$$\mathbf{b}^{\mathrm{tr}} = \mathbf{F}^{\mathrm{tr}}\cdot(\mathbf{F}^{\mathrm{tr}})^{\mathrm{t}} = \mathbf{F}\cdot^{n}\mathbf{C}_{\mathrm{p}}^{-1}\cdot\mathbf{F}^{\mathrm{t}} \tag{36}$$

the Kirchhoff stresses are obtained from the relations

$$\boldsymbol{\tau} = (1-\alpha)\hat{\boldsymbol{\tau}}, \text{ with } \hat{\boldsymbol{\tau}} = \hat{\boldsymbol{\tau}}^{\mathrm{vol}} + \hat{\boldsymbol{\tau}}^{\mathrm{dev}} \text{ and}$$

$$\hat{\boldsymbol{\tau}}^{\mathrm{vol}} = p\mathbf{g}^{\#}, p = K\ \ln\ J^{\mathrm{tr}}$$

$$\hat{\boldsymbol{\tau}}^{\mathrm{dev}} = \hat{\boldsymbol{\tau}}^{\mathrm{dev,tr}} - \frac{2G\Delta\lambda}{1-\alpha}\mathbf{n}, \text{ where } \hat{\boldsymbol{\tau}}^{\mathrm{dev,tr}} = G\ \mathrm{dev}\ \ln\mathbf{b}^{\mathrm{tr}}$$

$$\mathbf{n} = \frac{\hat{\boldsymbol{\tau}}^{\mathrm{dev}}}{\|\hat{\boldsymbol{\tau}}^{\mathrm{dev}}\|} \tag{37}$$

These sets of equations can be regarded as the counterpart of the relation (35) relative to the actual configuration.

3.2. Spectral decomposition

Upon using a spectral decomposition of the left elastic Cauchy–Green trial tensor and using the fact that due to isotropy $\mathbf{b}^{\mathrm{tr}}$ and $\boldsymbol{\tau}$ commute, we have

$$\mathbf{b}^{\mathrm{tr}} = \sum_{A=1}^{3}(\lambda_A^{\mathrm{tr}})^2\mathbf{m}_A \rightsquigarrow \boldsymbol{\tau} = \sum_{A=1}^{3}\beta_A\mathbf{m}_A \tag{38}$$

Here λ_A^{tr}, $\mathbf{m}_A$, $A = 1,2,3$ are the eigenvectors and eigenbasis of $\mathbf{b}^{\mathrm{tr}}$, respectively, and β_A, $A = 1,2,3$ are the principal values of the effective Kirchhoff stresses which by use of the vector/matrix notations

$$\underline{\varepsilon}^{\mathrm{tr}} := \begin{bmatrix} \ln\ \lambda_1^{\mathrm{tr}} \\ \ln\ \lambda_2^{\mathrm{tr}} \\ \ln\ \lambda_3^{\mathrm{tr}} \end{bmatrix}$$

$$\underline{\beta} := \begin{bmatrix} \beta_1 \\ \beta_2 \\ \beta_3 \end{bmatrix}$$

$$\underline{1} := \begin{bmatrix} 1 \\ 1 \\ 1 \end{bmatrix}$$

$$\underline{I}_3 := \begin{bmatrix} 1 & & \\ & 1 & \\ & & 1 \end{bmatrix}$$

$$\underline{I}_3^{\mathrm{dev}} := \underline{I}_3 - \frac{1}{3}\underline{1}\otimes\underline{1} \tag{39}$$

are obtained from the relations

$$\underline{\beta} = (1-\alpha)\hat{\underline{\beta}}, \text{ with } \hat{\underline{\beta}} = \hat{\underline{\beta}}^{\mathrm{vol}} + \hat{\underline{\beta}}^{\mathrm{dev}} \text{ and}$$

$$\hat{\underline{\beta}}^{\mathrm{vol}} = p\underline{1}, p = K\underline{1}\cdot\underline{\varepsilon}^{\mathrm{tr}}$$

$$\hat{\underline{\beta}}^{\mathrm{dev}} = \hat{\underline{\beta}}^{\mathrm{dev,tr}} - \frac{2G\Delta\lambda}{1-\alpha}\underline{\nu}, \text{ where } \hat{\underline{\beta}}^{\mathrm{dev,tr}} = 2G\underline{I}_3^{\mathrm{dev}}\cdot\underline{\varepsilon}^{\mathrm{tr}}$$

$$\underline{\nu} = \frac{\hat{\underline{\beta}}^{\mathrm{dev}}}{\|\hat{\underline{\beta}}^{\mathrm{dev}}\|} \tag{40}$$

These sets of equations can be regarded as the counterpart of the relations (35) and (37) in the principal directions. Note, that the above structure for the principal Kirchhoff stresses is identical to the geometric linear theory, see e.g. Simo [28].

3.3. Local iteration: two level algorithm

The two unknowns $\underline{x} = [\Delta\lambda,\alpha]^{\mathrm{t}}$ appearing in Eq. (40) are obtained from a nonlinear system of equations $\underline{r} = [r_1,r_2]^{\mathrm{t}} = \underline{0}$, where

$$r_1 = \|\hat{\underline{\beta}}^{\mathrm{dev,tr}}\| - \frac{2G\Delta\lambda}{1-\alpha} - \sqrt{\frac{2}{3}}(Y_0 + Q[q[\Delta\lambda]]) \tag{41a}$$

$$r_2 = -\alpha + {}^n\alpha + \frac{\Delta\lambda}{S(1-\alpha)^m} \frac{1}{2}\left(\frac{(Q+Y_0)^2}{3G} + \frac{p^2}{K}\right)\mathscr{T}[q[\Delta\lambda]] \tag{41b}$$

Here Eq. (41a) expresses the yield constraint and Eq. (41b) is obtained from the update scheme (32c) for the damage variable. A further constraint—which can lead to severe numerical difficulties—arises from the fact, that the variables contained in the vector $\underline{x}$ are restricted to lower and upper bounds a_i, b_i, $i = 1,2$. In particular we have $0 \leqslant \Delta\lambda < \infty$ and ${}^n\alpha \leqslant \alpha < 1$. We are therefore confronted with the following problem:

$$\text{Find } \underline{x} \in \mathbb{R}^2, \text{ such that } \underline{r}[\underline{x}] = \underline{0}, \quad a_i \leq x_i \leq b_i \quad i = 1,2 \tag{42}$$

If the starting point $\underline{x}^{(k=0)}$ is close enough to the solution point (assuming that it exists) the problem (42) can be solved iteratively with a Newton method

$$\underline{x}^{(k+1)} = \underline{x}^{(k)} - [\underline{J}^{(k)}]^{-1}\underline{r}^{(k)} \quad k = 0,1,2,\ldots \tag{43}$$

where the Jacobian

$$\underline{J} = \frac{\partial \underline{r}}{\partial \underline{x}} = \begin{bmatrix} \frac{\partial r_1}{\partial x_1} & \frac{\partial r_1}{\partial x_2} \\ \frac{\partial r_2}{\partial x_1} & \frac{\partial r_2}{\partial x_2} \end{bmatrix} \tag{44}$$

is required at each iteration point.

However, the superior local convergence property of the Newton method does not necessarily imply a good global convergence property in the case of improper starting values, see Johansson et al. [20] for a numerical example. Therefore, in order to gain more control and robustness of the iteration process a two-level strategy is adopted, whereby the two-dimensional problem (42) is solved by a sequence of one-dimensional problems. This allows the advantages of various one-dimensional solution schemes to be combined, e.g. the superior global convergence properties of a bisection method or a pegasus method, respectively (see e.g. Engelin–Müllges and Reuter [30]), with the superior local convergence property of a Newton method.

The iteration scheme is explained as follows [20]: firstly, for given (fixed) x_2 we use the one-dimensional iteration $x_1^{(k+1)} = x_1^{(k)} + \Delta x_1^{(k)}$, $k = 0,1,2,..$ until the condition $r_1[x_1^{(k)}, x_2] = 0$ is satisfied. However, the solution

$$x_1[x_2] = \arg\{r_1[x_1[x_2], x_2] = 0\} \tag{45}$$

in general does not satisfy the second condition $r_2[x_1[x_2], x_2] = 0$ so that an additional (outer) iteration $x_2^{(k+1)} = x_2^{(k)} + \Delta x_2^{(k)}$, $k = 0,1,2,. .$ becomes necessary. The basic idea consists now in determining a solution $x_1[x_2]$ according to Eq. (45) whenever x_2 is modified. In this manner the two-dimensional problem, Eq. (42), is converted into a sequence of one-dimensional problems.

In Table 1 the algorithm is summarized. For determination of the increment Δx_i, $i = 1,2$ several choices are possible:

- Bisection method: here the increment is obtained simply by

$$\Delta x_i^{(k)} = \tfrac{1}{2}(x_i^{\min} - x_i^{(k)}), \quad x_i^{\max} = x_i^{(k)}, \quad \text{if } r_i(x_i^{(k)}) \cdot r_i(x_i^{\max}) > 0$$

$$\Delta x_i^{(k)} = \tfrac{1}{2}(x_i^{\max} - x_i^{(k)}), \quad x_i^{\min} = x_i^{(k)}, \quad \text{else} \tag{46}$$

- Newton method: in this case the increment is calculated according to

$$\Delta x_i^{(k)} = -\left[\frac{\mathrm{d}r_i^{(k)}}{\mathrm{d}x_i}\right]^{-1} r_i^{(k)} \tag{47}$$

thus requiring the derivative of the residual r_i. For $i = 2$ we have

$$\frac{\mathrm{d}r_2}{\mathrm{d}x_2} = \frac{\partial r_2}{\partial x_2} + \frac{\partial r_2}{\partial x_1} \cdot \frac{\mathrm{d}x_1}{\mathrm{d}x_2}$$

Table 1
Two-level algorithm for nonlinear two-dimensional problem

FIND-ZERO(i):	
Object: determine x_i such that $r_1[x_1[x_2], x_2] = 0$ if $i = 1$ or $r_2[x_1[x_2], x_2] = 0$, if $i = 2$	
Algorithm:	
0. Initialize:	$k = 0$, $x_i^{(k=0)}$
1. Change level:	If ($i = 2$) call FIND-ZERO($i - 1$)
2. Residual:	r_i
3. Check tolerance:	If $\lvert r_i \rvert <$ tol, RETURN
4. Determine increment:	$\Delta x_i^{(k)}$
5. Update:	$x_i^{(k+1)} = x_i^{(k)} + \Delta x_i^{(k)}$, $k = k + 1$, GOTO 1

For evaluation of $\mathrm{d}x_1/\mathrm{d}x_2$ we exploit Step 1 of the algorithm in Table 1 which insures the condition

$$r_1[x_1[x_2],x_2] = 0 \rightsquigarrow \frac{\mathrm{d}r_1}{\mathrm{d}x_2} = \frac{\partial r_1}{\partial x_2} + \frac{\partial r_1}{\partial x_1}\frac{\mathrm{d}x_1}{\mathrm{d}x_2} = 0$$

The result for the derivative needed for the increment Eq. (47) is thus summarized as

$$i=1: \quad \frac{\mathrm{d}r_1}{\mathrm{d}x_1} = \frac{\partial r_1}{\partial x_1} \tag{48a}$$

$$i=2: \quad \frac{\mathrm{d}r_2}{\mathrm{d}x_2} = \frac{\partial r_2}{\partial x_2} - \frac{\partial r_2}{\partial x_1}\cdot\left[\frac{\partial r_1}{\partial x_1}\right]^{-1}\cdot\frac{\partial r_1}{\partial x_2} \tag{48b}$$

Observe, that the result (48b) is simply obtained by static condensation of the Jacobian, Eq. (44).

Alternative common iteration methods for one-dimensional problems are e.g. Regula Falsi, the pegasus method, and we refer to Engelin-Müllges [30] for the specific iteration schemes.

4. Equilibrium problem and associated derivatives

4.1. Weak formulation

Denoting $\boldsymbol{\varphi}$ as the configuration field at time ${}^{n+1}t$ for given parameters $\boldsymbol{\kappa} \in \mathscr{K}$ and using the notation $\langle \cdot, \cdot \rangle$ for the L_2 dual pairing on $\mathscr{B}_0$ of functions, vectors or tensor fields, the equilibrium problem as the classical weak form of momentum at time ${}^{n+1}t$ with spatial quantities reads

$$\text{Find } \boldsymbol{\varphi}: g[\boldsymbol{\varphi}] = \langle \boldsymbol{\tau}:\mathbf{d}_\delta \rangle - \bar{g} = 0 \ \forall \delta\mathbf{u} \text{ for given } \boldsymbol{\kappa} \in \mathscr{K} \tag{49}$$

Here the spatial rate of deformation tensor $\mathbf{d}_\delta$ induced by the virtual displacement $\delta\mathbf{u}$ is defined in the third part of Eq. (1), and $\bar{g} := \langle \bar{\mathbf{B}} \cdot \delta\mathbf{u} \rangle + \langle \bar{\mathbf{T}} \cdot \delta\mathbf{u} \rangle_{\partial_\sigma \mathscr{B}}$ designates the external part of the weak form for the case of dead loading with dual pairing $\langle \cdot, \cdot \rangle_{\partial_\sigma \mathscr{B}}$ on the boundary $\partial_\sigma \mathscr{B}$ and volume forces $\bar{\mathbf{B}}$ and surface forces $\bar{\mathbf{T}}$.

4.2. General concept: directional derivative and sensitivity operator

Before calculating derivatives of the weak form, Eq. (49), it is useful to consider the dependencies of some quantities w.r.t. the configuration $\boldsymbol{\varphi}$ and the material parameters $\boldsymbol{\kappa}$, e.g. from the definition of the deformation gradient $\mathbf{F} = \nabla_X \boldsymbol{\varphi}[\mathbf{X}, {}^{n+1}t, \boldsymbol{\kappa}]$ we can write $\mathbf{F} = \mathbf{F}[\boldsymbol{\varphi}[\boldsymbol{\kappa}]]$. However, the plastic part of the deformation gradient at time ${}^{n}t$ is *not* dependent on the actual configuration, and therefore we have $\mathbf{F}_\mathrm{p} = \mathbf{F}_\mathrm{p}[\boldsymbol{\kappa}]$. Both quantities define the left Cauchy–Green trial tensor, and thus

$$\mathbf{b}^{\mathrm{tr}} = \mathbf{b}^{\mathrm{tr}}[\boldsymbol{\varphi}[\boldsymbol{\kappa}],\boldsymbol{\kappa}] \rightsquigarrow \boldsymbol{\tau} = \boldsymbol{\tau}[\boldsymbol{\varphi}[\boldsymbol{\kappa}],\boldsymbol{\kappa}] \tag{50}$$

where the last relation for the Kirchhoff stresses is due to Eq. (37).

The above relations motivate the definitions of the following operators for any (scalar, vector or tensor valued) function $\mathbf{w}[\boldsymbol{\varphi}[\boldsymbol{\kappa}],\boldsymbol{\kappa}]$, which is dependent on the material parameters both implicitly via the configuration $\boldsymbol{\varphi}$ and explicitly: firstly, we introduce the standard *directional derivative (Gateaux) operator*

$$\partial_\Delta \mathbf{w} = \frac{\mathrm{d}\mathbf{w}}{\mathrm{d}\boldsymbol{\varphi}} \cdot \Delta\mathbf{u} = \frac{\mathrm{d}}{\mathrm{d}\epsilon}\{\mathbf{w}[\boldsymbol{\varphi}[\boldsymbol{\kappa}] + \epsilon\Delta\mathbf{u},\boldsymbol{\kappa}]\}_{\epsilon=0} \tag{51}$$

necessary for linearization of $\mathbf{w}$. Secondly, upon using the notation $\mathbf{v}_{\boldsymbol{\kappa}} = \mathrm{d}\boldsymbol{\varphi}/\mathrm{d}\boldsymbol{\kappa}$ we define a *sensitivity operator*

$$\partial_{\boldsymbol{\kappa}} \mathbf{w} = \partial^{\varphi}_{\boldsymbol{\kappa}} \mathbf{w} + \partial^{\mathrm{p}}_{\boldsymbol{\kappa}} \mathbf{w} \tag{52a}$$

where

$$\partial^{\varphi}_{\boldsymbol{\kappa}} \mathbf{w} = \frac{\mathrm{d}\mathbf{w}}{\mathrm{d}\boldsymbol{\varphi}} \cdot \mathbf{v}_{\boldsymbol{\kappa}} = \frac{\mathrm{d}}{\mathrm{d}\epsilon}\{\mathbf{w}[\boldsymbol{\varphi}[\boldsymbol{\kappa}] + \epsilon\mathbf{v}_{\boldsymbol{\kappa}},\boldsymbol{\kappa}]\}_{\epsilon=0} \tag{52b}$$

$$\partial^{\mathrm{p}}_{\boldsymbol{\kappa}} \mathbf{w} = \frac{\mathrm{d}\mathbf{w}(\cdot,\boldsymbol{\kappa})}{\mathrm{d}\boldsymbol{\kappa}} = \left(\lim_{\Delta\kappa_i \to 0} \frac{\mathbf{w}[\boldsymbol{\varphi}[\boldsymbol{\kappa}],\kappa_i + \Delta\kappa_i] - \mathbf{w}[\boldsymbol{\varphi}[\boldsymbol{\kappa}],\kappa_i]}{\Delta\kappa_i} \right)_{i=1}^{n_\mathrm{p}} \tag{52c}$$

which defines the total derivative $\partial_{\boldsymbol{\kappa}} \mathbf{w} = \mathrm{d}\mathbf{w}/\mathrm{d}\boldsymbol{\kappa}$. Note, that the term $\partial^{\varphi}_{\boldsymbol{\kappa}} \mathbf{w}$ has the same structure as $\partial_\Delta \mathbf{w}$ and can thus be obtained from the results for linearization by simply exchanging $\Delta\mathbf{u}$ with $\mathbf{v}_{\boldsymbol{\kappa}}$. The second term $\partial^{\mathrm{p}}_{\boldsymbol{\kappa}} \mathbf{w}$ basically excludes the implicit dependence of $\boldsymbol{\kappa}$ via the configuration at the actual time (or load) step ${}^{n+1}t$ and will subsequently be called the *partial parameter derivative*. Applying the above concept to the Kirchhoff stresses we obtain

$$\partial_\Delta \boldsymbol{\tau} = \mathscr{L}^{\#}_\Delta \boldsymbol{\tau} + 2\mathrm{sym}(\boldsymbol{\tau} \cdot \mathbf{l}^{\mathrm{t}}_\Delta)$$

$$\text{where } \mathscr{L}^{\#}_\Delta \boldsymbol{\tau} = 2\frac{\partial \boldsymbol{\tau}}{\partial \mathbf{g}^\flat} : \frac{1}{2}\mathscr{L}^\flat_\Delta \mathbf{g}^\flat = \mathbb{c} : \mathbf{d}_\Delta \tag{53a}$$

$$\partial_{\boldsymbol{\kappa}} \boldsymbol{\tau} = \mathscr{L}^{\#}_{\boldsymbol{\kappa}} \boldsymbol{\tau} + 2\mathrm{sym}(\boldsymbol{\tau} \cdot \mathbf{l}^{\mathrm{t}}_{\boldsymbol{\kappa}}) + \partial^{\mathrm{p}}_{\boldsymbol{\kappa}} \boldsymbol{\tau}$$

$$\text{where } \mathscr{L}^{\#}_{\boldsymbol{\kappa}} \boldsymbol{\tau} = 2\frac{\partial \boldsymbol{\tau}}{\partial \mathbf{g}^\flat} : \frac{1}{2}\mathscr{L}^\flat_{\boldsymbol{\kappa}} \mathbf{g}^\flat = \mathbb{c} : \mathbf{d}_{\boldsymbol{\kappa}} \tag{53b}$$

Here the spatial rate of deformation tensors $\mathbf{d}_\Delta$ and $\mathbf{d}_{\boldsymbol{\kappa}}$ induced by the linearization displacement $\Delta\mathbf{u}$ and configuration sensitivity $\mathbf{v}_{\boldsymbol{\kappa}}$, respectively, are defined in Eq.

(1). Furthermore, $\mathbb{c} := 2\partial\boldsymbol{\tau}/\partial\mathbf{g}^{\flat}$ is the fourth-order algorithmic spatial operator, and as alluded to above, the partial parameter derivative $\partial^{\mathrm{p}}_{\boldsymbol{\kappa}}\boldsymbol{\tau}$ excludes the implicit dependence of $\boldsymbol{\kappa}$ via the configuration $\boldsymbol{\varphi}$. Finally, upon using the relations

$$\partial_{\Delta}\mathbf{d}_{\delta} = -\mathrm{sym}(\mathbf{g}^{\flat}\cdot\mathbf{l}_{\delta}\cdot\mathbf{l}_{\Delta})$$

$$\partial_{\boldsymbol{\kappa}}\mathbf{d}_{\delta} = -\mathrm{sym}(\mathbf{g}^{\flat}\cdot\mathbf{l}_{\delta}\cdot\mathbf{l}_{\boldsymbol{\kappa}}) \tag{54}$$

we obtain the associated derivatives of the weak form as

$$\partial_{\Delta}g[\boldsymbol{\varphi}] = \langle(\mathbb{c}:\mathbf{d}_{\Delta}):\mathbf{d}_{\delta} + \mathbf{l}_{\Delta}\cdot\boldsymbol{\tau}:\mathbf{d}_{\delta}\rangle$$

$$\partial_{\boldsymbol{\kappa}}g[\boldsymbol{\varphi}] = \langle(\mathbb{c}:\mathbf{d}_{\boldsymbol{\kappa}}):\mathbf{d}_{\delta} + \mathbf{l}_{\boldsymbol{\kappa}}\cdot\boldsymbol{\tau}:\mathbf{d}_{\delta} + \partial^{\mathrm{p}}_{\boldsymbol{\kappa}}\boldsymbol{\tau}:\mathbf{d}_{\delta}\rangle \tag{55}$$

The first term is used for computation of an increment $\Delta\mathbf{u}$ within a Newton iteration step for iterative solution of the weak form, and the second term is used for computation of the configuration sensitivity $\mathbf{v}_{\boldsymbol{\kappa}}$ within an iteration step for minimization of some least-squares functional.

The next task consists in determination of the algorithmic spatial tangent operator $\mathbb{c}$ and the partial parameter derivative of Kirchhoff stresses $\partial^{\mathrm{p}}_{\boldsymbol{\kappa}}\boldsymbol{\tau}$, consistent with the integration scheme of Section 3.

4.3. Spatial algorithmic tangent operator

For the Kirchhoff stress tensor with structure of the right side of Eq. (38) the spatial algorithmic tangent operator $\mathbb{c}$ of Eq. (53) is obtained as (see e.g. Simo [28])

$$\mathbb{c} = \sum_{A=1}^{3}\sum_{B=1}^{3}\frac{\mathrm{d}\beta_A}{\mathrm{d}\varepsilon^{\mathrm{tr}}_B}\mathbf{m}_A\otimes\mathbf{m}_B + \sum_{A=1}^{3}2\beta_A\frac{\mathrm{d}\mathbf{m}_A}{\mathrm{d}\mathbf{g}^{\flat}} \tag{56}$$

where the expression for $\mathrm{d}\mathbf{m}_A/\mathrm{d}\mathbf{g}^{\flat}$ is presented in Simo [28]. The starting point for determination of the quantities $\mathrm{d}\beta_A/\mathrm{d}\varepsilon^{\mathrm{tr}}_B$ is the representation (40). Using vector notation we have

$$\begin{aligned}\frac{\mathrm{d}\underline{\beta}}{\mathrm{d}\underline{\varepsilon}^{\mathrm{tr}}} &= (1-\alpha)\frac{\mathrm{d}}{\mathrm{d}\underline{\varepsilon}^{\mathrm{tr}}}(\hat{\underline{\beta}}^{\mathrm{vol}} + \hat{\underline{\beta}}^{\mathrm{dev,tr}})\\ &\quad - (\hat{\underline{\beta}}^{\mathrm{vol}} + \hat{\underline{\beta}}^{\mathrm{dev,tr}})\otimes\frac{\mathrm{d}\alpha}{\mathrm{d}\underline{\varepsilon}^{\mathrm{tr}}}\\ &\quad - 2G\left(\underline{\nu}\otimes\frac{\mathrm{d}\Delta\lambda}{\mathrm{d}\underline{\varepsilon}^{\mathrm{tr}}} + \Delta\lambda\frac{\mathrm{d}\underline{\nu}}{\mathrm{d}\underline{\varepsilon}^{\mathrm{tr}}}\right)\end{aligned} \tag{57}$$

For determination of $\mathrm{d}\Delta\lambda/\mathrm{d}\underline{\varepsilon}^{\mathrm{tr}}$ and $\mathrm{d}\alpha/\mathrm{d}\underline{\varepsilon}^{\mathrm{tr}}$ we consider the local problem (41) as an implicit function and conclude

$$\begin{aligned}&\underline{r}[\underline{\varepsilon}^{\mathrm{tr}},\underline{x}[\underline{\varepsilon}^{\mathrm{tr}}]] = \underline{0} \rightsquigarrow \frac{\mathrm{d}\underline{r}}{\mathrm{d}\underline{\varepsilon}^{\mathrm{tr}}} = \frac{\partial\underline{r}}{\partial\underline{\varepsilon}^{\mathrm{tr}}} + \frac{\partial\underline{r}}{\partial\underline{x}}\frac{\mathrm{d}\underline{x}}{\mathrm{d}\underline{\varepsilon}^{\mathrm{tr}}} = \underline{0}\\ &\qquad\qquad \rightsquigarrow \frac{\mathrm{d}\underline{x}}{\mathrm{d}\underline{\varepsilon}^{\mathrm{tr}}} = -\underline{J}^{-1}\frac{\partial\underline{r}}{\partial\underline{\varepsilon}^{\mathrm{tr}}}\end{aligned} \tag{58}$$

where $\underline{J}$ is the Jacobian, Eq. (44). Upon defining

$$\begin{bmatrix}\delta_{11} & \delta_{12}\\ \delta_{21} & \delta_{22}\end{bmatrix} = \frac{1}{\det\,\underline{J}}\begin{bmatrix}-2GJ_{22} & J_{12}h\\ 2GJ_{21} & J_{11}h\end{bmatrix}$$

$$\text{where } h = \frac{\Delta\lambda}{(1-\alpha)^m}\,\frac{\mathscr{T}p}{S} \tag{59}$$

the following results are obtained after some algebra

$$\frac{\mathrm{d}\Delta\lambda}{\mathrm{d}\underline{\varepsilon}^{\mathrm{tr}}} = \delta_{11}\underline{\nu} + \delta_{12}\underline{1}$$

$$\frac{\mathrm{d}\alpha}{\mathrm{d}\underline{\varepsilon}^{\mathrm{tr}}} = \delta_{21}\underline{\nu} + \delta_{22}\underline{1} \tag{60}$$

Furthermore, employing the results

$$\frac{\mathrm{d}\underline{\nu}}{\mathrm{d}\underline{\varepsilon}^{\mathrm{tr}}} = \frac{2G}{\|\hat{\underline{\beta}}^{\mathrm{dev,tr}}\|}(\underline{I}_3^{\mathrm{dev}} - \underline{\nu}\otimes\underline{\nu})$$

$$\frac{\mathrm{d}}{\mathrm{d}\underline{\varepsilon}^{\mathrm{tr}}}(\hat{\underline{\beta}}^{\mathrm{vol}} + \hat{\underline{\beta}}^{\mathrm{dev,tr}}) = K\underline{1}\otimes\underline{1} + 2G\underline{I}_3^{\mathrm{dev}} \tag{61}$$

expands the expression (57) as

$$\frac{\mathrm{d}\underline{\beta}}{\mathrm{d}\underline{\varepsilon}^{\mathrm{tr}}} = \alpha_1\underline{1}\otimes\underline{1} + \alpha_2\underline{I}_3^{\mathrm{dev}} + \alpha_3\underline{\nu}\otimes\underline{\nu} + \alpha_4\underline{\nu}\otimes\underline{1} + \alpha_5\underline{1}\otimes\underline{\nu}$$

where $\alpha_1 = (1-d)K - p\delta_{22}$

$$\alpha_2 = 2G\left(1 - \alpha - \frac{2G\Delta\lambda}{\|\hat{\underline{\beta}}^{\mathrm{dev,tr}}\|}\right)$$

$$\alpha_3 = \frac{(2G)^2\Delta\lambda}{\|\hat{\underline{\beta}}^{\mathrm{dev,tr}}\|} - 2G\delta_{11} - \|\hat{\underline{\beta}}^{\mathrm{dev,tr}}\|\delta_{21}$$

$$\alpha_4 = -2G\delta_{12} - \|\hat{\underline{\beta}}^{\mathrm{dev,tr}}\|\delta_{22}$$

$$\alpha_5 = -p\delta_{21} \tag{62}$$

Thus, due to the nonsymmetry of the above expression the algorithmic tangent operator (56) exhibits also a nonsymmetric structure contrary to the hyperelastic–plastic tangent operator (30). This is a consequence of the complete coupling between elasticity and damage

Table 2
Large strain problems formulated in principal directions: partial parameter sensitivity for the Kitchhoff stresses and the parameter sensitivity of right Cauchy–Green plastic strain (material independent part)

(a) Partial parameter sensitivity for Kitchhoff stresses (pre-processing) input: ${}^{n}\mathbf{C}_{\mathrm{p}}^{-1}$	
$\partial^{\mathrm{p}}_{\boldsymbol{\kappa}}\mathbf{b}^{\mathrm{tr}} =$	$\mathscr{L}^{\#}_{\boldsymbol{\kappa}}\mathbf{b}^{\mathrm{tr}} = \mathbf{F}\cdot\partial^{n}_{\boldsymbol{\kappa}}\mathbf{C}_{\mathrm{p}}^{-1}\cdot\mathbf{F}^{\mathrm{t}}$
$\partial^{\mathrm{p}}_{\boldsymbol{\kappa}}\varepsilon^{\mathrm{tr}}_{A} =$	$\frac{1}{2}\frac{1}{(\lambda^{\mathrm{tr}}_{A})^{2}}\mathbf{m}_{A}:\partial^{\mathrm{p}}_{\boldsymbol{\kappa}}\mathbf{b}^{\mathrm{tr}},\quad A=1,2,3$
for $\partial^{\mathrm{p}}_{\boldsymbol{\kappa}}\beta_{A}$:	see material-dependent part in Table 3
$\partial^{\mathrm{p}}_{\boldsymbol{\kappa}}\mathbf{m}_{A} =$	$\partial_{\mathbf{b}^{\mathrm{tr}}}\mathbf{m}_{A}:\partial^{\mathrm{p}}_{\boldsymbol{\kappa}}\mathbf{b}^{\mathrm{tr}},\quad A=1,2,3$ (for $\partial_{\mathbf{b}^{\mathrm{tr}}}\mathbf{m}_{A}$ see Ref. [31])
$\partial^{\mathrm{p}}_{\boldsymbol{\kappa}}\boldsymbol{\tau} =$	$\sum_{A=1}^{3}\partial^{\mathrm{p}}_{\boldsymbol{\kappa}}\beta_{A}\mathbf{m}_{A}+\sum_{A=1}^{3}\beta_{A}\partial^{\mathrm{p}}_{\boldsymbol{\kappa}}\mathbf{m}_{A}$
(b) Parameter sensitivity for the internal strain-like variables (post-processing) input: ${}^{n}\mathbf{C}_{\mathrm{p}}^{-1}$, $\mathbf{v}_{\boldsymbol{\kappa}}$	
$\mathbf{l}_{\boldsymbol{\kappa}} =$	$\partial_{\boldsymbol{\kappa}}\mathbf{F}\cdot\mathbf{F}^{-1}$, $\partial_{\boldsymbol{\kappa}}\mathbf{F}=\frac{\partial\mathbf{v}_{\boldsymbol{\kappa}}}{\partial\mathbf{X}}$
$\partial_{\boldsymbol{\kappa}}\mathbf{b}^{\mathrm{tr}} =$	$\mathscr{L}^{\#}_{\boldsymbol{\kappa}}\mathbf{b}^{\mathrm{tr}}+2\mathrm{sym}(\mathbf{l}_{\boldsymbol{\kappa}}\cdot\mathbf{b}^{\mathrm{tr}})$, where $\mathscr{L}^{\#}_{\boldsymbol{\kappa}}\mathbf{b}^{\mathrm{tr}}=\mathbf{F}\cdot\partial^{n}_{\boldsymbol{\kappa}}\mathbf{C}_{\mathrm{p}}^{-1}\cdot\mathbf{F}^{\mathrm{t}}$
$\partial_{\boldsymbol{\kappa}}\varepsilon^{\mathrm{tr}}_{A} =$	$\frac{1}{2}\frac{1}{(\lambda^{\mathrm{tr}}_{A})^{2}}\mathbf{m}_{A}:\partial_{\boldsymbol{\kappa}}\mathbf{b}^{\mathrm{tr}}$
for $\partial_{\boldsymbol{\kappa}}\varepsilon^{\mathrm{el}}_{A}$:	see material-dependent part in Table 3
$\partial_{\boldsymbol{\kappa}}\lambda^{\mathrm{el}^{2}}_{A} =$	$2\lambda^{\mathrm{el}^{2}}_{A}\partial_{\boldsymbol{\kappa}}\varepsilon^{\mathrm{el}}_{A},\quad A=1,2,3$
$\partial_{\boldsymbol{\kappa}}\mathbf{m}_{A} =$	$\partial_{\mathbf{b}^{\mathrm{tr}}}\mathbf{m}_{A}:\partial_{\boldsymbol{\kappa}}\mathbf{b}^{\mathrm{tr}},\quad A=1,2,3$ (for $\partial_{\mathbf{b}^{\mathrm{tr}}}\mathbf{m}_{A}$ see Ref. [31])
$\partial_{\boldsymbol{\kappa}}\mathbf{b}^{\mathrm{el}} =$	$\sum_{A=1}^{3}(\partial_{\boldsymbol{\kappa}}\lambda^{\mathrm{el}^{2}}_{A}\mathbf{m}_{A}+\lambda^{\mathrm{el}^{2}}_{A}\partial_{\boldsymbol{\kappa}}\mathbf{m}_{A})$
$\partial_{\boldsymbol{\kappa}}\mathbf{C}_{\mathrm{p}}^{-1} =$	$-2\mathrm{sym}(\mathbf{F}^{-1}\cdot\partial_{\boldsymbol{\kappa}}\mathbf{F}\cdot{}^{n}\mathbf{C}_{\mathrm{p}}^{-1})+\mathbf{F}^{-1}\cdot\partial_{\boldsymbol{\kappa}}\mathbf{b}^{\mathrm{el}}\cdot\mathbf{F}^{-\mathrm{t}}$

as introduced in Eq. (6), and is different to the presentation by Steinmann et al. [15], where only the elastic isochoric part of the free energy is coupled to damage.

4.4. Partial parameter derivative of Kirchhoff stresses

4.4.1. General remarks

Similar as to the material operator $\mathbb{c}$, Eq. (56), the partial parameter derivative of Kirchhoff stresses appearing in Eq. (53) consists of two parts (see e.g. [27]):

$$\frac{\partial^{\mathrm{p}}\boldsymbol{\tau}}{\partial\boldsymbol{\kappa}}=\sum_{A=1}^{3}\mathbf{m}_{A}\otimes\frac{\partial^{\mathrm{p}}\beta_{A}}{\partial\boldsymbol{\kappa}}+\sum_{A=1}^{3}\beta_{A}\frac{\partial^{\mathrm{p}}\mathbf{m}_{A}}{\partial\boldsymbol{\kappa}} \tag{63}$$

The expressions necessary for determination of $\partial^{\mathrm{p}}\boldsymbol{\tau}/\partial\boldsymbol{\kappa}$ are summarized in Tables 2 and 3, respectively. In Table 2 those terms are recalled from Mahnken and Stein in [27], which are valid for any model formulated in principal directions. Table 3 contains the expressions resulting from the specific model formulation in Section 2.

From the results of a *pre-processing part* in Tables 2 and 3, respectively, it can be seen that calculation of $\partial^{\mathrm{p}}\boldsymbol{\tau}/\partial\boldsymbol{\kappa}$ also involves expressions for the parameter derivative of state variables $\mathrm{d}^{n}q/\mathrm{d}\boldsymbol{\kappa}$, $\mathrm{d}^{n}\alpha/\mathrm{d}\boldsymbol{\kappa}$, $\mathrm{d}^{n}\mathbf{C}_{\mathrm{p}}^{-1}/\mathrm{d}\boldsymbol{\kappa}$ at the *previous time step*. Therefore, after having solved the linear problem in the second equation of Eq. (55) for $\mathbf{v}_{\boldsymbol{\kappa}}$, it becomes necessary to determine $\mathrm{d}^{n+1}q/\mathrm{d}\boldsymbol{\kappa}$, $\mathrm{d}^{n+1}\alpha/\mathrm{d}\boldsymbol{\kappa}$, $\mathrm{d}^{n+1}\mathbf{C}_{\mathrm{p}}^{-1}/\mathrm{d}\boldsymbol{\kappa}$ at the actual time step in a *post-processing part*, in order to make them available for the next time step.

As already mentioned, all expressions of Table 2 are derived and explained in Mahnken and Stein [27]. In what follows, we will briefly comment on the expressions of Table 3.

4.4.2. Pre-processing

The starting point for determination of $\partial^{\mathrm{p}}\beta_{A}/\partial\boldsymbol{\kappa}$ in Eq. (63) is the representation (40). Using vector notation analogously to Eq. (57) we have

$$\begin{aligned}\frac{\partial^{\mathrm{p}}\underline{\beta}}{\partial\boldsymbol{\kappa}}&=(1-\alpha)\frac{\partial^{\mathrm{p}}}{\partial\boldsymbol{\kappa}}(\underline{\hat{\beta}}^{\mathrm{vol}}+\underline{\hat{\beta}}^{\mathrm{dev,tr}})\\&\quad-(\underline{\hat{\beta}}^{\mathrm{vol}}+\underline{\hat{\beta}}^{\mathrm{dev,tr}})\otimes\frac{\partial^{\mathrm{p}}\alpha}{\partial\boldsymbol{\kappa}}\\&\quad-2G\left(\underline{\nu}\otimes\frac{\partial^{\mathrm{p}}\Delta\lambda}{\partial\boldsymbol{\kappa}}+\Delta\lambda\frac{\partial^{\mathrm{p}}\underline{\nu}}{\partial\boldsymbol{\kappa}}\right)\end{aligned} \tag{64}$$

The determination of $\partial^{\mathrm{p}}\Delta\lambda/\partial\boldsymbol{\kappa}$ and $\partial^{\mathrm{p}}\alpha/\partial\boldsymbol{\kappa}$ is contained in the following result: we consider the local problem (41) as an implicit function and derive

$$\begin{aligned}\underline{r}[\boldsymbol{\kappa},\underline{x},{}^{n}q,{}^{n}\alpha,\underline{\varepsilon}^{\mathrm{tr}}]=\underline{0}\rightsquigarrow\frac{\mathrm{d}\underline{r}}{\mathrm{d}\boldsymbol{\kappa}}&=\frac{\overline{\partial}\underline{r}}{\partial\boldsymbol{\kappa}}+\frac{\partial\underline{r}}{\partial\underline{x}}\frac{\mathrm{d}\underline{x}}{\mathrm{d}\boldsymbol{\kappa}}=\underline{0}\\\rightsquigarrow\frac{\mathrm{d}\underline{x}}{\mathrm{d}\boldsymbol{\kappa}}&=-\underline{J}^{-1}\frac{\overline{\partial}\underline{r}}{\partial\boldsymbol{\kappa}}\end{aligned} \tag{65}$$

for the total derivative. Here $\underline{J}$ is the Jacobian (44) and the notation

$$\frac{\overline{\partial}\underline{r}}{\partial\boldsymbol{\kappa}} = \frac{\partial\underline{r}}{\partial\boldsymbol{\kappa}} + \frac{\partial\underline{r}}{\partial^n q}\frac{\mathrm{d}^n q}{\mathrm{d}\boldsymbol{\kappa}} + \frac{\partial\underline{r}}{\partial^n \alpha}\frac{\mathrm{d}^n \alpha}{\mathrm{d}\boldsymbol{\kappa}} + \frac{\partial\underline{r}}{\partial\underline{\varepsilon}^{\mathrm{tr}}}\frac{\mathrm{d}\underline{\varepsilon}^{\mathrm{tr}}}{\mathrm{d}\boldsymbol{\kappa}} \tag{66}$$

has been used. The result for $\partial^{\mathrm{p}}\underline{x}/\partial\boldsymbol{\kappa}$ is then obtained from Eq. (65) by exchanging $\mathrm{d}\underline{\varepsilon}^{\mathrm{tr}}/\mathrm{d}\boldsymbol{\kappa}$ with $\partial^{\mathrm{p}}\underline{\varepsilon}^{\mathrm{tr}}/\partial\boldsymbol{\kappa}$ and is given in the pre-processing part of Table 3. Using this result, the final expression for $\partial^{\mathrm{p}}\beta_A/\partial\boldsymbol{\kappa}$ is obtained from Eq. (64) and is also summarized in the pre-processing part of Table 3.

4.4.3. Post-processing

For determination of $\mathrm{d}^{n+1}q/\mathrm{d}\boldsymbol{\kappa}$, $\mathrm{d}^{n+1}\alpha/\mathrm{d}\boldsymbol{\kappa}$, $\mathrm{d}^{n+1}\mathbf{C}_{\mathrm{p}}^{-1}/\mathrm{d}\boldsymbol{\kappa}$ in Table 3 firstly $\mathrm{d}\Delta\lambda/\mathrm{d}\boldsymbol{\kappa}$ and $\mathrm{d}\alpha/\mathrm{d}\boldsymbol{\kappa}$ are calculated from Eq. (65). The detailed expressions are given in the post-processing part of Table 3. Then, from Eq. (32b) we have

$$\frac{\mathrm{d}q}{\mathrm{d}\boldsymbol{\kappa}} = \frac{\mathrm{d}^n q}{\mathrm{d}\boldsymbol{\kappa}} + \sqrt{\frac{2}{3}}\frac{\mathrm{d}\Delta\lambda}{\mathrm{d}\boldsymbol{\kappa}} \tag{67}$$

For determination of $\mathrm{d}^{n+1}\mathbf{C}_{\mathrm{p}}^{-1}/\mathrm{d}\boldsymbol{\kappa}$ in Table 2 we need $\mathrm{d}\underline{\varepsilon}^{\mathrm{el}}/\mathrm{d}\boldsymbol{\kappa}$, where

$$\underline{\varepsilon}^{\mathrm{el}} = \underline{\varepsilon}^{\mathrm{tr}} - \frac{\Delta\lambda}{1-\alpha}\underline{\nu} \tag{68}$$

(see Mahnken and Stein [27], Proposition 5.8). Differentiation of Eq. (68) w.r.t. $\boldsymbol{\kappa}$ yields after some algebra the result presented in the post-processing part of Table 3.

5. Plane sheet with two notches

A plane sheet with two notches is considered with geometry as shown in Fig. 1. The material of the specimen is a mild steel, Baustahl St52 due to the German regulations for construction steel. This example was investigated experimentally in the context of the german research network Sonderforschungsbereich 319 (SFB 319): 'Stoffgesetze für das inelastische Verhalten metallischer Werkstoffe—Entwicklung und Anwendung' University of Braunschweig, Germany. In particular spatially distributed data were obtained with an optical method, a *grating method* (see Andresen and Hübner [24] and Bergmann et al. [25]). To this end a grating is positioned on the surface as shown in Fig. 2. This is photographed with a digital camera at consecutive observation states during the displacement controlled experiment with load sizes according to Table 4. Finally the data are analyzed digitally, thus leading to highly resolved spatially distributed data for displacement fields.

The numerical simulation of this plane stress example is performed with a plane stress element presented by Steinmann et al. [32]. This formulation allows the incorporation of general 3D constitutive

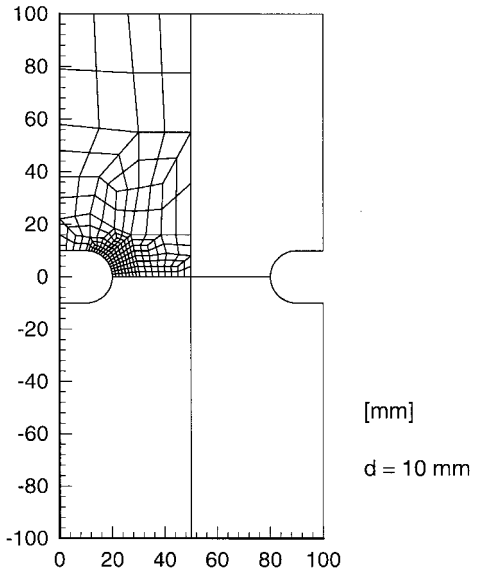

Fig. 1. Plane sheet with two notches: geometry and discretization.

models without any plane stress constraints. Instead, the constraint $\tau_{33}=0$ is satisfied in a weak sense. In our simulation a quadratic nine node element has been used. The spatial discretization of the sample is shown in Fig. 1.

The material is assumed to be elastoplastic J_2-flow theory, combined with isotropic damage and nonlinear isotropic hardening according to Section 2. Integration is performed with the algorithm described in Section 3 in $N = 205$ load steps.

The input data for the identification process consists of displacements in x- and/or y-direction at different, arbitrarily chosen points near the notch region, so that the total number of data at each observation state is $n_{x\mathrm{dat}}=51$. The total number of observation states is $n_{\mathrm{tdat}}=7$ according to Table 4.

The object is to identify the six parameters Y_0, b, c, S, m, ϵ_1 of Eq. (19) which characterize the inelastic behavior of the material. Two elastic parameters were pre-determined as $E = 20600$ kN/cm^2 and $\nu=0.3$ for Young's modulus and Poisson's ratio, respectively, and the parameter ϵ_1 was set to 0.01. In this respect, the following objective function of least-squares type is examined:

$$f(\boldsymbol{\kappa}) = \frac{1}{2}\sum_{i=1}^{n_{\mathrm{tdat}}=7}\sum_{j=1}^{n_{x\mathrm{dat}}=51}(u_{ij}-\bar{u}_{ij})^2 + \frac{1}{2}\sum_{i=1}^{n_{\mathrm{tdat}}=7} w_i(F_i-\bar{F}_i)^2 \rightarrow \min_{\boldsymbol{\kappa}} \tag{69}$$

where here u_{ij} denotes the displacement in either x- or

Table 3
Large strain multiplicative von Mises elastoplasticity formulated in principal directions: algorithmic constants for the partial parameter sensitivity of the stress variables (pre-processing) and the parameter sensitivity of internal strain-like variables (post-processing)

Input for pre-processing: $\partial^n_{\boldsymbol{\kappa}} q$, $\partial^n_{\boldsymbol{\kappa}} \alpha$, replace $\partial_{\boldsymbol{\kappa}} \underline{\varepsilon}^{\mathrm{tr}}$ by $\partial^{\mathrm{p}}_{\boldsymbol{\kappa}} \underline{\varepsilon}^{\mathrm{tr}}$ from Table 2, part (a)
Input for post processing: $\partial^n_{\boldsymbol{\kappa}} q$, $\partial^n_{\boldsymbol{\kappa}} \alpha$, $\partial_{\boldsymbol{\kappa}} \underline{\varepsilon}^{\mathrm{tr}}$ from Table 2, part (b)
Effective principal stresses:
$\partial_{\boldsymbol{\kappa}} p = K \mathrm{tr}(\partial_{\boldsymbol{\kappa}} \underline{\varepsilon}^{\mathrm{tr}}) \rightsquigarrow \partial_{\boldsymbol{\kappa}} \hat{\underline{\beta}}^{\mathrm{vol}} = \partial_{\boldsymbol{\kappa}} p \underline{1}, \quad \partial_{\boldsymbol{\kappa}} \hat{\underline{\beta}}^{\mathrm{dev,tr}} = 2G \, \mathrm{dev}(\partial_{\boldsymbol{\kappa}} \underline{\varepsilon}^{\mathrm{tr}})$
Normal vector:

$$\partial_{\boldsymbol{\kappa}} \underline{\nu} = \frac{1}{\| \hat{\underline{\beta}}^{\mathrm{dev,tr}} \|} [\underline{I}_3^{\mathrm{dev}} - \underline{\nu} \otimes \underline{\nu}] \partial_{\boldsymbol{\kappa}} \hat{\underline{\beta}}^{\mathrm{dev,tr}}$$

Residual r_1:

$$\partial_{\boldsymbol{\kappa}} Q = \begin{bmatrix} 0 \\ cq \exp(-bq) \\ 1 - \exp(-bq) \\ 0 \\ 0 \\ 0 \\ 0 \end{bmatrix}, \partial_{\boldsymbol{\kappa}} Y_0 = \begin{bmatrix} 1 \\ 0 \\ 0 \\ 0 \\ 0 \\ 0 \\ 0 \end{bmatrix}, \frac{\partial Q}{\partial^n q} = cb \exp(-bq)$$

$$\bar{\partial}_{\boldsymbol{\kappa}} r_1 = \underline{\nu} : \partial_{\boldsymbol{\kappa}} \hat{\underline{\beta}}^{\mathrm{dev,tr}} - \sqrt{\frac{2}{3}} \left(\partial_{\boldsymbol{\kappa}} Y_0 + \partial_{\boldsymbol{\kappa}} Q + \frac{\partial Q}{\partial^n q} \partial^n_{\boldsymbol{\kappa}} q \right)$$

Residual r_2:

$$\partial_{\boldsymbol{\kappa}} S = \begin{bmatrix} 0 \\ 0 \\ 0 \\ 1 \\ 0 \\ 0 \\ 0 \end{bmatrix}, \partial_{\boldsymbol{\kappa}} m = \begin{bmatrix} 0 \\ 0 \\ 0 \\ 0 \\ 1 \\ 0 \\ 0 \end{bmatrix}, \partial_{\boldsymbol{\kappa}} \mathscr{T} = \begin{bmatrix} 0 \\ 0 \\ 0 \\ 0 \\ 0 \\ \dfrac{-6(q-\varepsilon_1)}{(\epsilon_2-\epsilon_1)^2} + \dfrac{6(q-\epsilon_1)}{(\epsilon_2-\epsilon_1)^3} \\ \dfrac{-6(q-\epsilon_1)^2}{(\epsilon_2-\epsilon_1)^3} + \dfrac{6(q-\epsilon_1)^3}{(\epsilon_2-\epsilon_1)^4} \end{bmatrix} \; if \, \epsilon_1 < q < \epsilon_2 \, else \, \partial_{\boldsymbol{\kappa}} \mathscr{T} = \underline{0}$$

$$\frac{\partial \mathscr{T}}{\partial^n q} = \frac{6(q-\epsilon_1)(\epsilon_2 - q)}{(\epsilon_2 - \epsilon_1)^3}, \quad \bar{\partial}_{\boldsymbol{\kappa}} \mathscr{T} = \frac{\partial \mathscr{T}}{\partial^n q} \partial^n_{\boldsymbol{\kappa}} q + \partial_{\boldsymbol{\kappa}} \mathscr{T}$$

$$\bar{\partial}_{\boldsymbol{\kappa}} r_2 = \partial^n_{\boldsymbol{\kappa}}\alpha + \frac{\Delta\lambda}{(1-\alpha)^m}\frac{1}{2}\left(\frac{(Q+Y_0)^2}{3G}+\frac{p^2}{K}\right)\left(\frac{1}{S}\bar{\partial}_{\boldsymbol{\kappa}}\mathscr{T} - \frac{\mathscr{T}}{S^2}\partial_{\boldsymbol{\kappa}} S\right) + \frac{\Delta\lambda}{(1-\alpha)^m}\frac{\mathscr{T}}{S}\frac{1}{2}\left(\frac{Q+Y_0}{3G}\partial_{\boldsymbol{\kappa}}(Q+Y_0)+\frac{p}{K}\partial_{\boldsymbol{\kappa}} p\right) - \frac{\Delta\lambda}{(1-\alpha)^m}\frac{\mathscr{T}}{S}\frac{1}{2}\left(\frac{(Q+Y_0)^2}{3G}+\frac{p^2}{K}\right)\log(1-\alpha)\partial_{\boldsymbol{\kappa}} m$$

$$\partial_{\boldsymbol{\kappa}}\Delta\lambda = \frac{-1}{\det J}(\bar{\partial}_{\boldsymbol{\kappa}} r_1 J_{22} - \bar{\partial}_{\boldsymbol{\kappa}} r_2 J_{12}), \quad \partial_{\boldsymbol{\kappa}}\alpha = \frac{-1}{\det J}(\bar{\partial}_{\boldsymbol{\kappa}} r_2 J_{11} - \bar{\partial}_{\boldsymbol{\kappa}} r_1 J_{21})$$

If pre-processing then

$$h_1 = 1 - \alpha - \frac{2G\Delta\lambda}{\|\hat{\underline{\beta}}^{\mathrm{dev,tr}}\|}$$

$$H^{\,1}_{\boldsymbol{\kappa}} = \frac{2G\Delta\lambda}{\|\hat{\underline{\beta}}^{\mathrm{dev,tr}}\|}\mathbf{n}{:}\partial_{\boldsymbol{\kappa}}\hat{\underline{\beta}}^{\mathrm{dev,tr}} - \|\hat{\underline{\beta}}^{\mathrm{dev,tr}}\|\partial_{\boldsymbol{\kappa}}\alpha - 2G\partial_{\boldsymbol{\kappa}}\Delta\lambda$$

$$H^{\,2}_{\boldsymbol{\kappa}} = (1-\alpha)\partial_{\boldsymbol{\kappa}} p - p\partial_{\boldsymbol{\kappa}}\alpha$$

$$\partial_{\boldsymbol{\kappa}}\hat{\underline{\beta}} = h_1\partial_{\boldsymbol{\kappa}}\hat{\underline{\beta}}^{\mathrm{dev,tr}} + H^{\,1}_{\boldsymbol{\kappa}}\underline{\nu} + H^{\,2}_{\boldsymbol{\kappa}}\underline{1}$$

else

$$\partial_{\boldsymbol{\kappa}} q = \partial^n_{\boldsymbol{\kappa}} q + \sqrt{\frac{2}{3}}\partial_{\boldsymbol{\kappa}}\Delta\lambda$$

$$H^{\,3}_{\boldsymbol{\kappa}} = \frac{\Delta\lambda}{\|\hat{\underline{\beta}}^{\mathrm{dev,tr}}\|}\mathbf{n}{:}\partial_{\boldsymbol{\kappa}}\hat{\underline{\beta}}^{\mathrm{dev,tr}} - \frac{\partial_{\boldsymbol{\kappa}}\Delta\lambda}{1-\alpha} - \frac{\Delta\lambda\partial_{\boldsymbol{\kappa}}\alpha}{(1-\alpha)^2}$$

$$\partial_{\boldsymbol{\kappa}}\underline{\varepsilon}^{\mathrm{el}} = \mathrm{dev}\,\partial_{\boldsymbol{\kappa}}\underline{\varepsilon}^{\mathrm{tr}} + H^{\,3}_{\boldsymbol{\kappa}}\underline{\nu} - \frac{\Delta\lambda}{(1-\alpha)\|\hat{\underline{\beta}}^{\mathrm{dev,tr}}\|}\partial_{\boldsymbol{\kappa}}\hat{\underline{\beta}}^{\mathrm{dev,tr}}$$

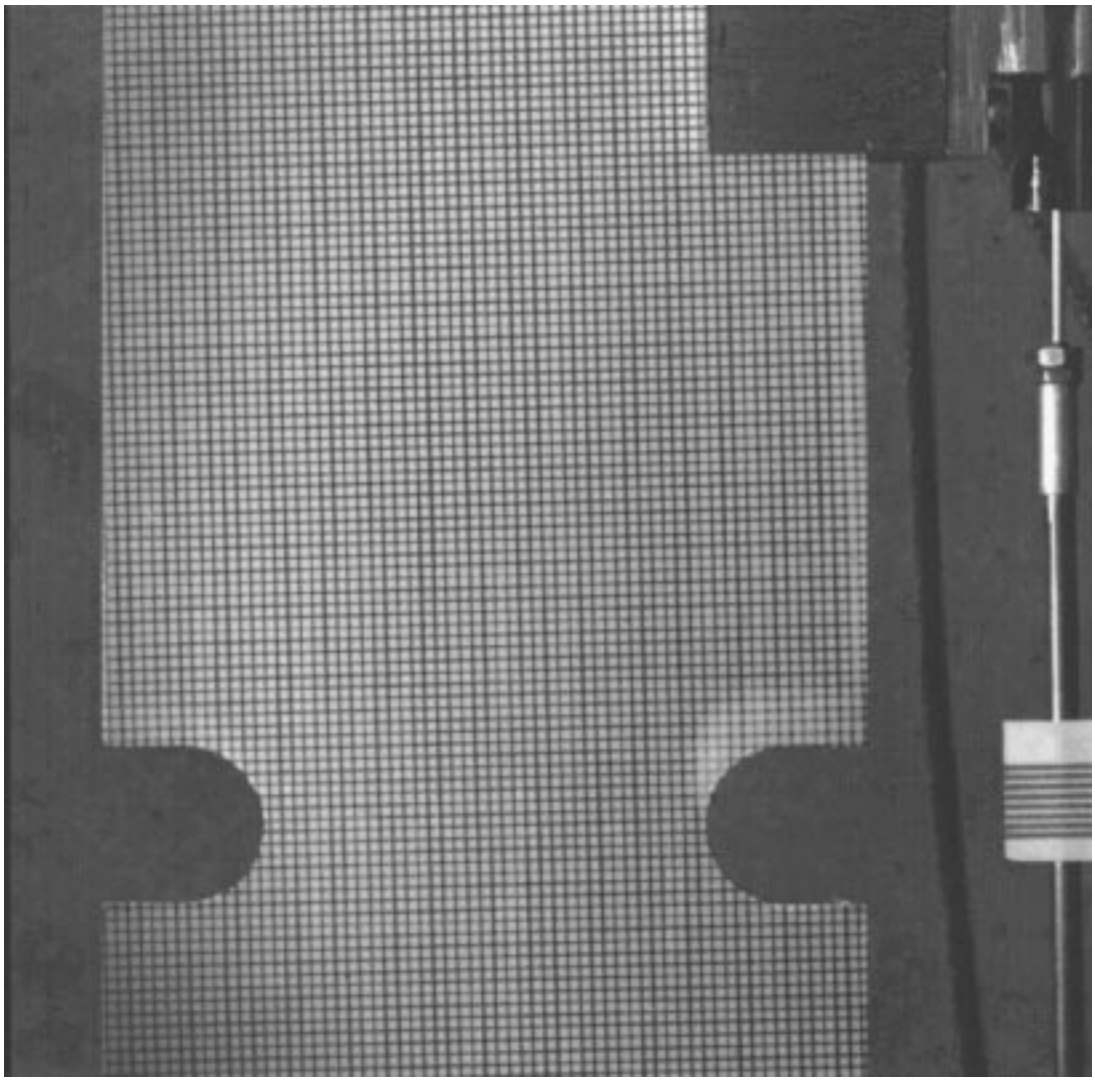

Fig. 2. Plane sheet with two notches: photography of the sample with grating on the surface.

y-direction and F_j the total tension load acting on the specimen. w is a weighting factor and is set to 2×10^{-8}. For minimization of the least-squares functional (69) an algorithm due to Bertsekas [33] is used, where the iteration matrix is obtained from the update rule for the BFGS formula. Further details of the algorithm are explained in e.g. Mahnken and Stein [26,27].

Table 4
Plane sheet with two notches: sizes of displacement at the top of the sample at different states of optical observation

NLST	1	6	10	15	18	21	28
Load size (mm)	0.0	0.44	1.0	2.0	3.0	4.0	5.3

The starting point and the results of the optimization process for the material parameters are given in Table 5. The result has been obtained after 18 iteration steps. For comparison also the results of [27] are recalled, which are obtained from identification of a different experiment with the same material, however from a different production charge. This difference in the specimen causes some type of scattering and is regarded as the main reason for the differences in the results. A larger amount of data would become necessary in order to apply a stochastic approach to this type of model uncertainty [34,35].

In Fig. 3 the total load versus the upper displacement is depicted for both for simulation and experiment, which reveals a very good agreement. In Figs. 4–6 we compare the contours for the displacements u

Table 5
Plane sheet with two notches: starting and obtained values for the material parameters of a mild steel Baustahl St52

	Starting	Solution	Ref. [27]
Y_0 (N/mm^2)	300.0	351.17	360.26
b	10.0	7.223	3.95
c (N/mm^2)	800.0	355.8	416.51
S	10.0	8.068	–
m	0.4	0.499	–
ϵ_1	0.4	0.405	–

and v, respectively, at the observation states $NSLT = 6$ and $NSLT = 28$ of Table 4 in the grating region. Again, a very substantial agreement between experimental and simulated data is observed.

6. Summary

In this work a model for plasticity coupled to damage formulated in the plastic intermediate configuration has been proposed. The formulation is based on complete coupling between the elastic part of the free energy function and the damage variable. As a consequence an evolution equation for the damage variable is obtained which is proportional to the accumulated plastic strain rate and which is in accordance with the analytical investigations for ductile growth of voids by Rice and Tracey [17]. Furthermore it preserves an increase of damage evolution with increasing triaxiality ratio, which is in agreement with the experimental observation that the measured ductility at fracture decreases as the triaxiality ratio increases [2,3]. In this respect the formulation is regarded as an important modification to the presentation by Steinmann et al. [15], where only the elastic isochoric part of the free energy function is coupled to damage.

Furthermore, issues of thermodynamic consistency, continuous tangent operator, and algorithmic tangent operator have been discussed. Due to the complete coupling of elasticity and damage in the free energy function, the algorithmic tangent operator becomes non-symmetric. Furthermore, for the discretized constitutive problem a robust iteration scheme with a two-level algorithm is proposed. A gradient based optimization algorithm is used for minimizing the associative least-squares functional for parameter identification, and to this end the associated sensitivity analysis con-

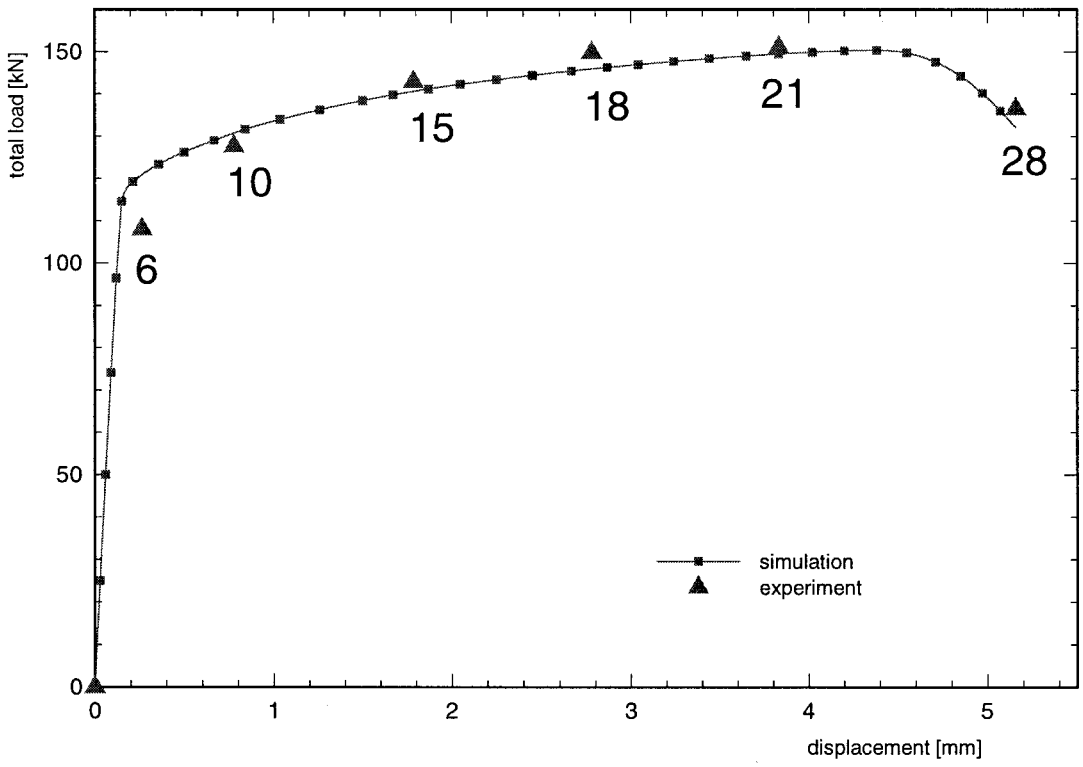

Fig. 3. Plane sheet with two notches: load versus displacement for simulation and experiment.

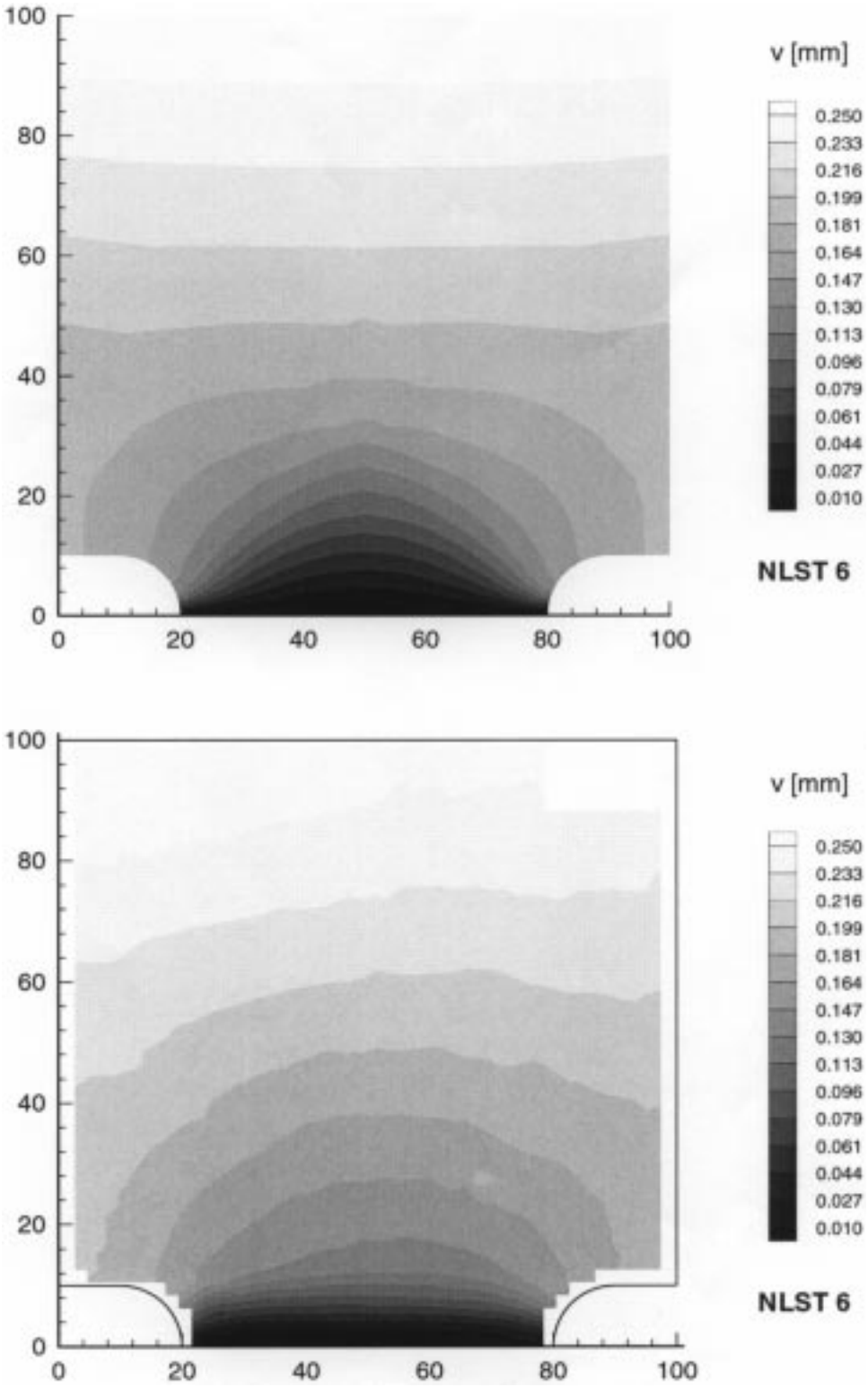

Fig. 4. Plane sheet with two notches: contours of displacements v for simulation (top) and experiment (bottom) at observation state 6 in the grating region.

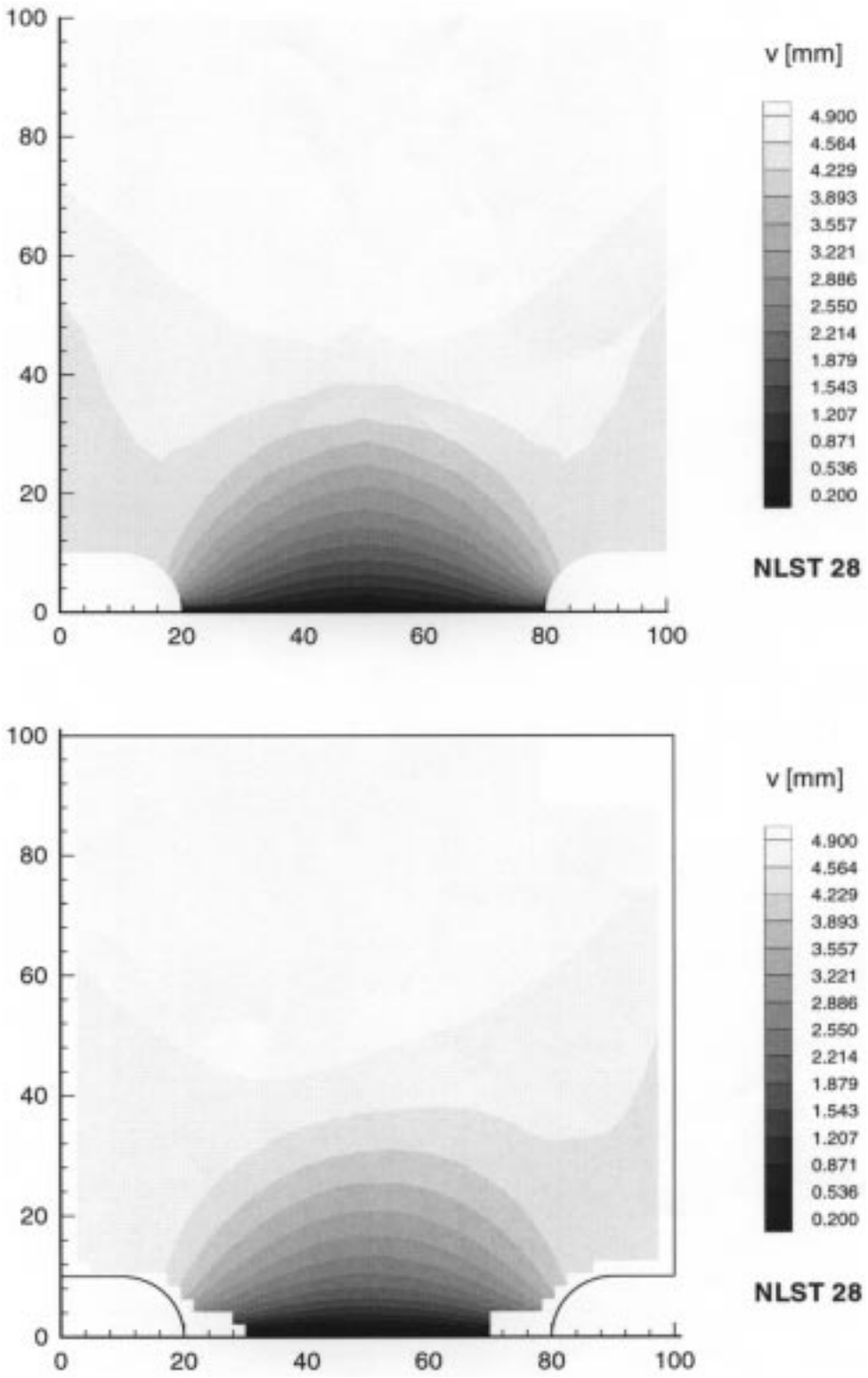

Fig. 5. Plane sheet with two notches: contours of displacements v for simulation (top) and experiment (bottom) at observation state 28 in the grating region.

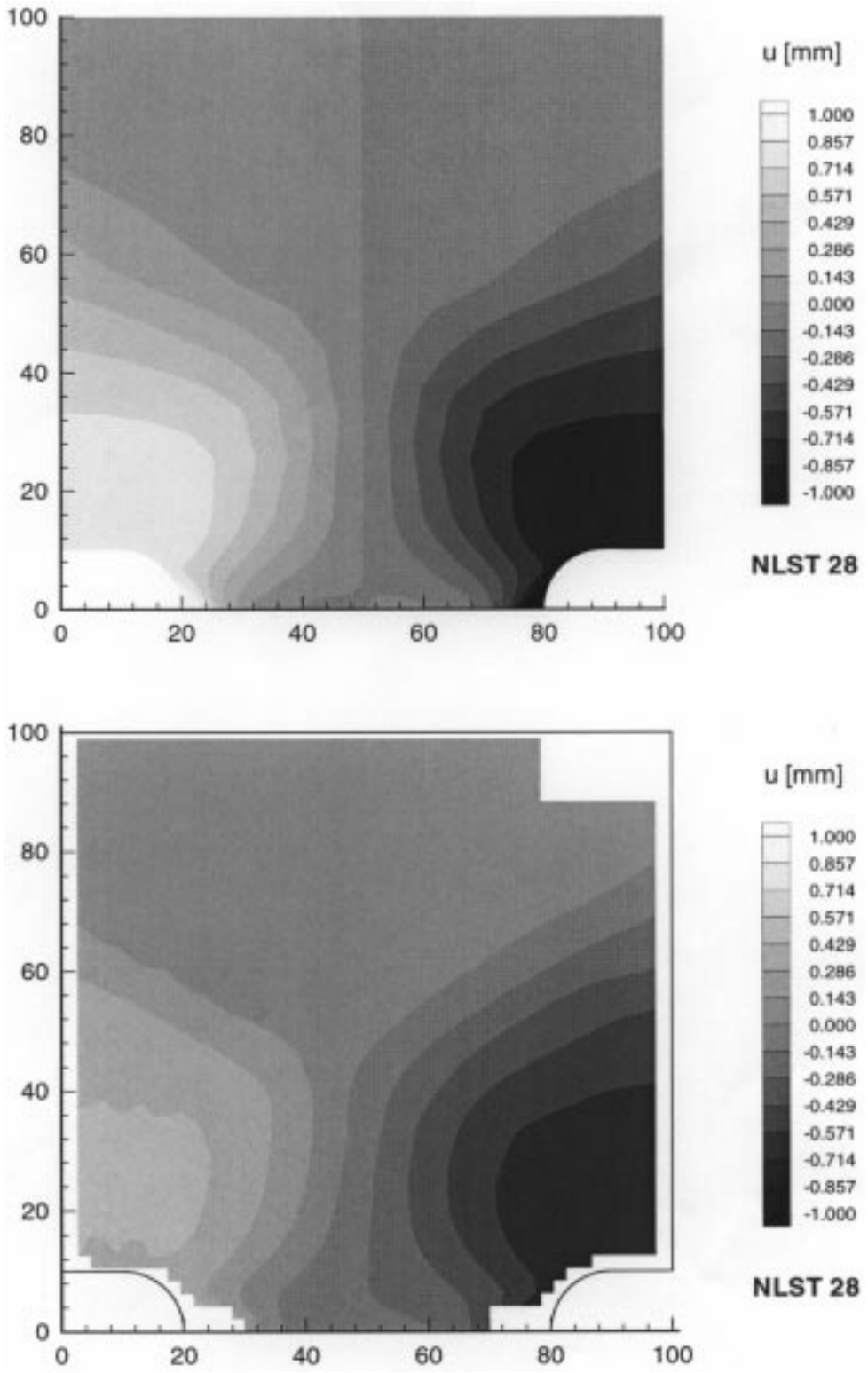

Fig. 6. Plane sheet with two notches: contours of displacements u for simulation (top) and experiment (bottom) at observation state 28 in the grating region.

sistent with the integration scheme has been described. In the example experimental data obtained with a grating method were used, in order to determine the material parameters of the model, thus leading to very good agreement between numerical simulation and experimental observations.

Acknowledgements

This work was performed in the context of the German research network Sonderforschungsbereich 319 (SFB 319): 'Stoffgesetze für das inelastische Verhalten metallischer Werkstoffe—Entwicklung und Anwendung'. In this respect the cooperative collaboration with the following institutes and associated persons from the University of Braunschweig is gratefully acknowledged: Professor Dr-Ing. U. Peil and Dipl.-Ing. S. Dannemeier from the Institut für Stahlbau, who performed the experiment; Professor Dr-Ing. R. Ritter and Dipl.-Ing. H. Friebe from the Institut für experimentelle Mechanik, who did the digital photographs. The financial support for this research was provided by the Deutsche Forschungsgemeinschaft and is gratefully acknowledged.

References

[1] Lemaitre J. A course on damage mechanics, 2nd ed. Berlin: Springer, 1996.
[2] Thomason PF. Ductile fracture of metals. Oxford: Pergamon Press, 1990.
[3] Hancock JW, Mackenzi AC. On the mechanisms of ductile failure in the high-strength steels subjected to multiaxial stress-states. J Mech Phys Solids 1976;24:147–69.
[4] Gurson AL. Continuum theory of ductile rupture by void nucleation and growth—I. Yield criteria and flow rules for porous ductile media. Engng Mater Technol 1977;99:2–15.
[5] Tvergaard V. Influence of voids on shear band instabilities under plane strain conditions. Int J Fract 1981;17:389–407.
[6] Tvergaard V, Needleman A. Analysis of the cup–cone fracture in a round tensile bar. Acta Metall 1984;32:157–69.
[7] Bennani B, Picart P, Oudin J. Some basic finite element analysis of microvoid nucleation, growth and coalescencs. Engng Comput 1993;10:409–21.
[8] Steglich D, Brocks W. Micromechanical modelling of the behaviour of ductile materials including particles. Comput Mater Sci 1997;9:7–17.
[9] Mahnken R. Aspects on the finite element implementation of the Gurson model including parameter identification (submitted).
[10] Kachanov LM. Time to the rupture process under creep conditions. TVZ Akad Nauk SSR Otd Tech Nauk 1958;8:26–31.
[11] Chaboche JL. Continuum damage mechanics: part I—general concepts. J Appl Mech 1988;55:59–72.
[12] Simo JC, Ju JW. Strain- and stress-based continuum damage models—I. Formulation. Int J Solids Struct 1987;23:821–40.
[13] Lemaitre J. Coupled elasto-plasticity and damage constitutive equations. Comput Meth Appl Mech Engng 1985;51:31–49.
[14] De Souza EA, Peric D, Owen DR. A model for elasto-plastic damage at finite strains: algorithmic issues and applications. Engng Comput 1994;11:257–81.
[15] Steinmann P, Miehe Ch, Stein E. Comparison of different finite deformation inelastic damage models within multiplicative plasticity for ductile materials. Int J Comput Mech 1993;13:458–74.
[16] Miehe Ch. On the representation of Prandtl–Reuss tensors within the framework of multiplicative elastoplasticity. Int J Plast 1994;10:609–21.
[17] Rice, Tracey. On the ductile enlargement of voids in triaxial stress fields. J Mech Phys Solids 1969;17:201–17.
[18] Weber G, Anand L. Finite deformation constitutive equations and a time integration procedure for isotropic, hyperelastic–viscoplastic solids. Comput Meth Appl Mech Engng 1990;79:173–202.
[19] Eterovic AL, Bathe KJ. A hyperelastic based large strain elasto-plastic constitutive formulation with combined isotropic-kinematic hardening using the logarithmic stress and strain measures. Int J Numer Meth Engng 1990;30:1099–114.
[20] Johansson M, Mahnken R, Runesson K. Efficient integration for generalized viscoplasticity coupled to damage, Int J Numer Meth Engng (in press).
[21] Banks HT, Kunisch K. Estimation techniques for distributed parameter systems. Boston: Birkhäuser, 1989.
[22] Bui HD. Inverse problems in the mechanics of materials, an introduction. Boca Raton, FL: CRC Press, 1994.
[23] Bui HD, Tanaka M, editors. Inverse problems in engineering mechanics. Rotterdam: Balkema, 1994.
[24] Andresen K, Hübner B. Calculation of strain from an object grating on a Reseau film by a correlation method. Exp Mech 1992;32:96–101.
[25] Bergmann D, Galanulis K, Ritter R. Optical field methods for 3D-deformation measurement in fracture mechanics. In: Carpinteri A, editor. Size–Scale Effects in the Failure Mechanics of Materials and Structure. London: E & FN SPON, 1996. p. 524–536.
[26] Mahnken R, Stein E. A unified approach for parameter identification of inelastic material models in the frame of the finite element method. Comput Meth Appl Mech Engng 1996;136:225–58.
[27] Mahnken R, Stein E. Parameter identification for finite deformation elastoplasticity in principal directions. Comput Meth Appl Mech Engng 1997;147:17–39.
[28] Simo JC. Algorithms for static and dynamic multiplicative plasticity that preserve the classical return mapping schemes of the infinitesimal theory. Comput Meth Appl Mech Engng 1992;99:61–112.
[29] Steinmann P. 1997 Modellierung und Numerik duktiler Werkstoffe. Habilitation, Forschungs-und Seminarberichte aus dem Bereich der Mechanik der Universität Hannover, F97/1.

[30] Engelin-Müllges G, Reuter F. Formelsammlung zur numerischen Mathematik mit Standard-FORTRAN 77 Programmen. Mannheim: BI-Wissenschaftsverlag, 1988.
[31] Miehe C. Computation of isotropic tensor functions. Commun Appl Numer Meth 1993;9:889–96.
[32] Steinmann P, Betsch P, Stein E. FE plane stress analysis incorporating arbitrary 3D large strain constitutive models. Engng Comput 1997;14:175–201.
[33] Bertsekas DP. Projected Newton methods for optimization problems with simple constraints. SIAM J Con Opt 1982;20:221–46.
[34] Pugachew VS. Probability theory and mathematical statistics for engineers. Oxford: Pergamon Press, 1984.
[35] Stein E, Ohnimus S, Mahnken R. Adaptive modeling and computation of elastic and inelastic structures. In: Natke HG, Ben-Haim Y, editors. Uncertainty: Models and Measures, Proceedings of the International Workshop, Lamprecht, Germany, 22–24 July 1996. Chichester: Wiley, 1997.